Chapter 14 Molecular Tagging Velocimetry in Gases

Robert W. Pitz and Paul M. Danehy

To appear in

Optical Diagnostics for Reacting and Non-Reacting Flow: Theory and Practice

Edited by Adam Steinberg and Sukesh Roy

1. Introduction

1.1 What is MTV?

In molecular tagging velocimetry (MTV), the laser "tags" the gas molecules along the laser beam and the tagged molecules are tracked by time-of-flight to determine the gas velocity. For example, hydroxyl tagging velocimetry (HTV) is shown in Figs. 1 and 2. ArF excimer laser beams (11x11) are crossed in a plane in a Mach 2 wind tunnel and dissociate water molecules in the air flow into OH that is imaged by planar laser-induced fluorescence (LIF) from a 282-nm laser sheet (Fig. 1) [1, 2]. The displacements of the OH tag crossings are measured over a fixed time delay (2 μs) to determine the velocity in a 2D plane (Fig. 2 right, a 700 m/s vector is shown for reference) [2].

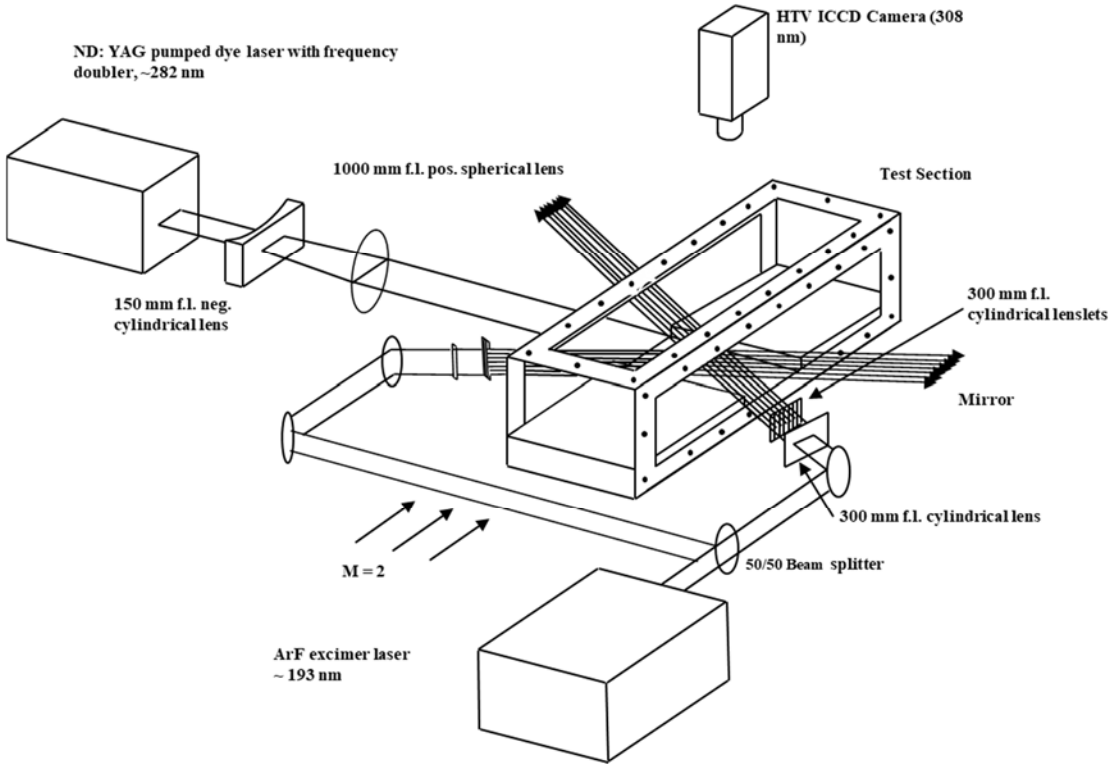

Fig. 1. Hydroxyl Tagging Velocimetry (HTV) in a Mach 2 wind tunnel [2].

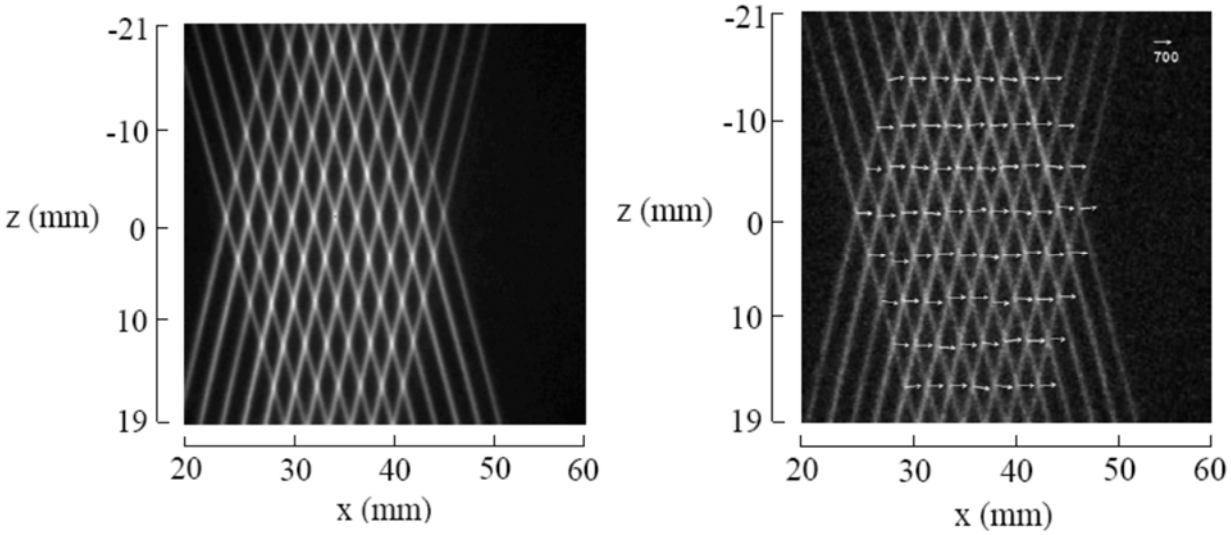

Fig. 2. HTV images taken in the freestream of a Mach 2 air flow at 0 µs (left) and 2 µs (right) to determine velocity (m/s) [2].

1.2 Need for Velocity Measurement without Particles

Most velocity techniques measure the gas velocity by seeding the gas with droplets or particles and measure the light scattering from the particles to determine the gas velocity [3]. Common particle-based velocity methods include particle-imaging-velocimetry (PIV), planar Doppler velocimetry (PDV) (alternately known as Doppler global velocimetry (DGV)), and laser Doppler velocimetry (LDV) [3]. Particle scattering velocity methods have the advantage of strong scattering signals but suffer some drawbacks. In high-speed flows, the particle velocity can differ from the gas velocity due to particle lag effects [4, 5]. As seen in Fig. 3, Huffman et al. [6] compared velocity measurements using PIV to Acetone MTV in the underexpanded jet flowfield finding serious particle lag effects in that the PIV failed to capture the velocity ahead and behind the normal shock even for PIV particles as small as 0.1 µm.

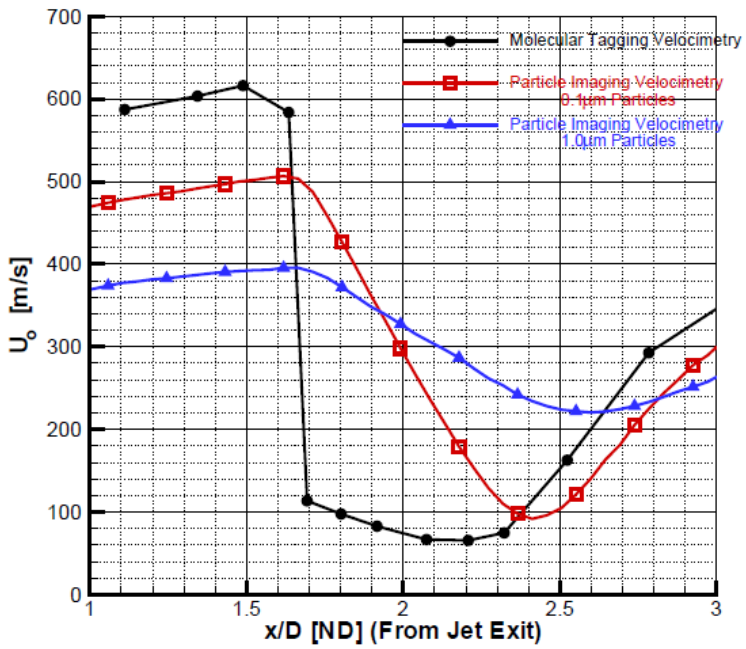

Figure 3. Comparison of velocity measured by acetone MTV and PIV on the centerline of an underexpanded jet flowfield created by a sonic jet [6].

In some facilities (i.e., large wind tunnels, rocket chambers/plumes, reciprocating internal combustion (IC) engines), it can be difficult to introduce particles, the particles quickly coat the windows [7] or the use of added particles may be prohibited, for example, because of contamination. Furthermore, particles can agglomerate which makes them heavier and less likely to follow flow streamlines. By directly measuring the velocity of the gas, MTV avoids all of these difficulties associated with particle velocity methods. Another favorable aspect of MTV compared to particle scattering techniques is that the fluorescent MTV signals are at a different wavelength than the laser reducing scattered light interference (e.g. near surfaces) that often occurs with particle scattering method (unless using fluorescent particles). However, MTV usually probes points, lines, and grids which make the spatial resolution generally worse than many particle-based 2D or even 3D measurement techniques such as PIV and PDV/DGV.

1.3 Basic Concepts in MTV

Molecular tagging velocimetry uses both "unseeded" and "seeded" methods [8]. In "unseeded" methods, the molecules are already contained in the gas flow to be tagged. Air is the most common gas and contains O_2, N_2, Ar, CO_2 and H_2O. A number of MTV methods create tags in air including air photolysis and recombination tracking (APART) [9], femtosecond laser electronic excitation tagging (FLEET) [10, 11], hydroxyl tagging velocimetry (HTV) [1, 2], two-photon H_2O photolysis [12-14], ozone tagging velocimetry (OTV) [15-17], and RELIEF [18-20]. Imidogen tagging velocimetry (ITV) measures velocity with an NH tag in nitrogen flows with trace water vapor or added hydrogen [21, 22]. Other "seeded" methods add molecules to the flow (acetone [23], biacetyl [24, 25], iodine [26], krypton [27, 28], sodium [29], nitric oxide [30-32], nitrogen dioxide [33-35], nitrous oxide [36, 37], and tert-butyl nitrate [38]) that are tagged to measure velocity.

Molecular tagging velocimetry methods are divided into "linear" and "non-linear" methods of laser excitation. Linear excitation methods "write" the tag lines with a one-photon process allowing longer tag lines [1, 2, 15-17, 21-25, 30-38]. Non-linear excitation methods "write" the tag line with multi-photon process that generally leads to shorter but more tightly focused tag lines allowing examination of small fluid flow features [9-14, 18-20, 26-29].

MTV methods are classified as "single-laser" and "multiple-laser" methods. Single-laser methods are generally simpler and less costly. In single-laser methods [10, 11, 22-26, 28, 30-32], a single laser writes the tag line and emission from excited state molecules in the displaced tag line allows it to imaged or "read". In multiple-laser methods, generally a second laser sheet is used image or "read" the tag line by planar LIF [1, 2, 9, 12-21, 27, 29, 33, 34, 36, 37]. Sometimes two laser lines are needed to "write" the tag line [18-20]. Two laser sheets are sometimes used to "read" the tag line at two time delays to remove errors associated with vibrations or alignment drift that would otherwise lead to measurement errors estimated to be as large as 28% of the total uncertainty in one experiment [32].

In MTV experiments, there is a tradeoff between measurement uncertainty and spatial resolution: longer time delays which improve accuracy and precision must be traded off against the larger displacement of the tagged fluid which effectively worsens the spatial resolution. Furthermore, if the time separation between camera acquisitions is too large and if the gas accelerates between the

images an incorrect velocity is obtained. In this case, theoretical and computational predictions of fluid displacement can be compared instead of velocity [39].

2. Single-Laser Methods

With single-laser methods, the laser excites molecules in a point, line, or grid inducing molecular fluorescence or phosphorescence whose emissive lifetime is long compared to the time scale of the flow (e.g. the laser beam diameter divided by the flow velocity). A gated intensified camera images the emitting molecules from the tag at different distances downstream allowing the gas velocity to be determined. If the lifetime is sufficiently long, multiple images can be acquired to measure acceleration [40]. When a laser beam is viewed as a line, a 1-velocity-component profile can be measured. In some cases, many lines can be illuminated in the flow allowing many velocity profiles to be simultaneously measured [Reference 30, Bathel]. Some non-linear techniques (e.g., FLEET, detailed in section 2.3) can generate signal from a small spot instead of a line. In this case, two (and even three) components of velocity can be measured with one detector [40-43]. Alternately, a pair or series of lines can be projected at different angles and two components of velocity can be measured at the grid points [10, 24, 44]. This method can be further extended too many crossing lines allowing field measurements of velocity as demonstrated below. While numerous molecules have been probed using single-laser methods, this section describes just a few instructive examples.

2.1. Biacetyl tagging velocimetry

To the authors' knowledge, the first MTV paper in gaseous flows noted in the literature is from Hiller et al. [25] who focused a pulsed dye laser into a 6 m/s nitrogen flow seeded with biacetyl molecules. A 5-ns duration YAG-pumped dye laser at 430 nm excited phosphorescence in the biacetyl. Successive exposures were recorded on a 100x100 pixel intensified photodiode array camera using separate laser pulses for each image. Figure 4 shows images resulting from this experiment from which velocity was determined by computing the displacement divided by the delay after the laser pulse. While the reported image quality and spatial resolution was low by today's standards, this initial experiment demonstrated a promising method for instantaneous (single-shot) velocity profile measurement.

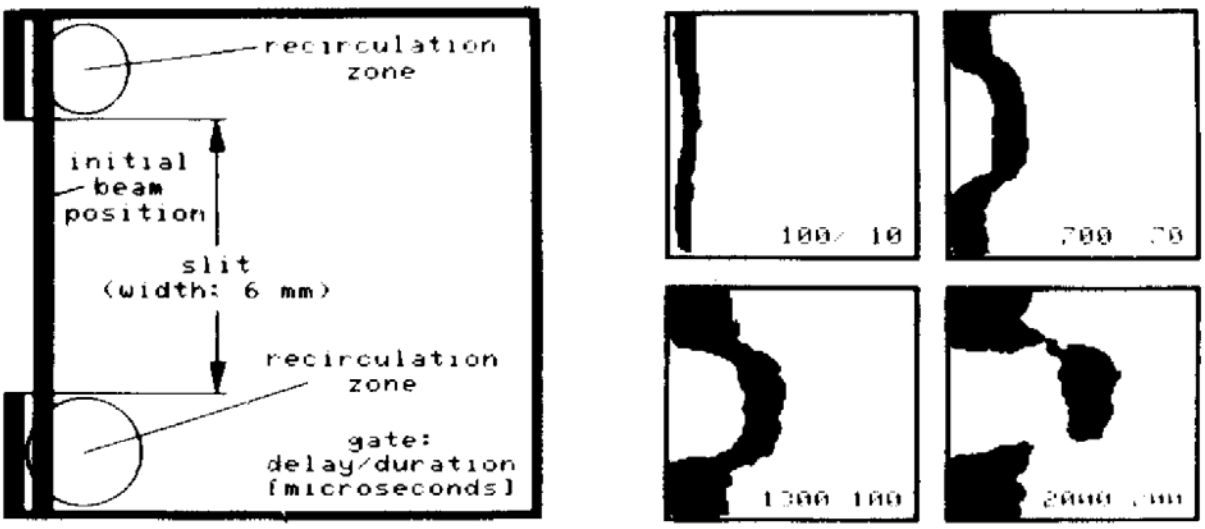

Figure 4. Biacetyl phosphorescence MTV in a nitrogen jet. Flow is from left to right. The bottom right of each figure shows the camera delay after laser pulse and the duration of the intensifier gate in microseconds [25].

A more advanced application of biacetyl phosphorescence MTV is from Stier and Koochesfahani [24] who applied biacetyl MTV to study the air intake of a non-reacting internal combustion engine. This was achieved by using a 308-nm XeCl excimer laser which is much more powerful than that used by Hiller et al. [25]. This higher power allowed multiple lines to be tagged simultaneously. The laser light was split into two paths and formed to generate a grid as shown in Figure 5, left. The flow is biacetyl seeded into nitrogen. Since oxygen quenches the phosphorescence, air cannot be used. This flow was injected into a quartz model engine (8.3 cm dia.) and interrogated by the laser that was transmitted through the quartz cylinder walls. A 512x512 pixel intensified camera acquired the reference (zero delay) and delayed images from which the velocity and vorticity fields were obtained as shown in Figure 6. The use of grid-excitation allowed a second velocity component to be measured and significantly increased the region of the flow measured. Furthermore, the use of the grid excitation reduced or eliminated a potential error in the single-line excitation MTV in which there is ambiguity in the origin of the delayed, tagged fluid since it originated from a uniformly tagged line [24, 32].

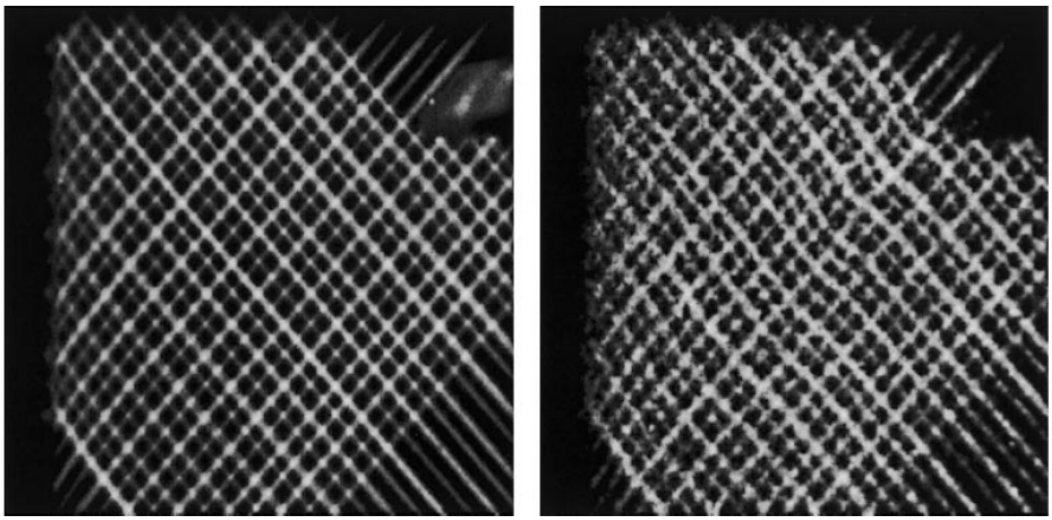

Figure 5. 20-shot averaged reference image (left) and instantaneous 50-μs delayed image (right) obtained during air intake of an internal combustion engine using single-laser biacetyl MTV. The field of view is 3 cm x 3 cm [24].

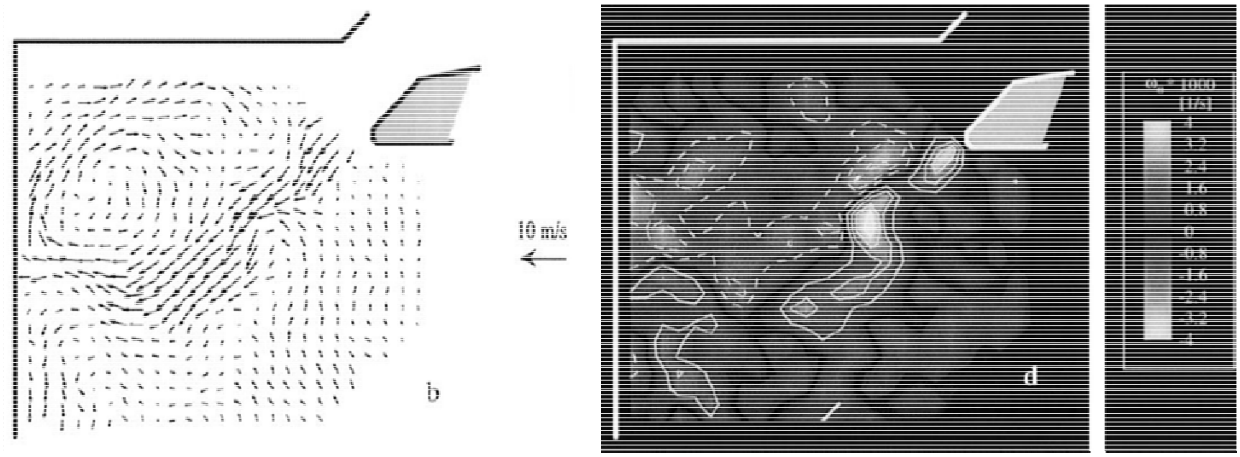

Figure 6. Instantaneous 2D velocity (left, b) and vorticity (right, d) fields obtained during air intake of an internal combustion as in Figure 4 [24].

2.2. Nitric oxide (NO) fluorescence tagging velocimetry

Nitric oxide is a naturally-occurring component of high-temperature air. In high-enthalpy wind tunnels such as shock tubes and arc-jets NO can be approximately 3% of the gas composition [45-47]. Alternately, since NO is relatively stable (in the absence of water vapor or O_2) it can be procured in a gas bottle and seeded into high-speed flow facilities, often operating with a balance of N_2 [48]. Since the fluorescence lifetime (1/e) of NO is ~ 200 ns, it can be used for single-laser velocimetry if the flow is fast enough to move appreciably in a few hundred ns (e.g. hypervelocity flows). This technique was first demonstrated by Danehy et al. [31] in a high-enthalpy free-piston shock tunnel containing naturally occurring NO produced by shock heating a 1.1% O_2, 98.9% N_2 mixture. A Nd:YAG pumped dye laser was used to generate light at 225 nm that was focused to excite a line of NO in the flow perpendicular to a flat plate. The technique was used to study a

laminar boundary layer and the flow separation forward of a blunt fin mounted perpendicular to a flat plate. Free piston shock tunnels move appreciably during operation, potentially causing a measurement error when comparing signal and reference (zero velocity) images. However, a small amount of fluorescence from the plate itself persisted in the delayed images (shown near the plate in Fig. 7) which allowed the location of the reference image to be determined. The reported measurement precision in this experiment was about 100 m/s (based on one standard deviation). Measurements were made as close as 0.2 mm from the wall. Images acquired with shorter delays after the laser pulse had smaller displacements while longer delays had more displacement but lower signal-to-noise ratio. An error analysis indicated that, for that experiment, the optimum delay was around 500 ns or about 2.5 NO fluorescence lifetimes. Advantages of this method are that NO was naturally occurring in this flow (no additional seeding required), the measurement was instantaneous (single-shot) and that the technique was relatively easy to implement with only a single laser and single camera required. Subsequent work extended the instrument to measure 25 velocity profiles simultaneously and to lower uncertainties by about a factor of 2 owing to various improvements including near-simultaneous acquisition of signal and reference images for every laser pulse using an interline transfer camera which defends against vibrations and laser pointing issues [32]. A limitation of the method is that it does not work well at higher densities required to simulate high Reynolds number flows since the fluorescence lifetime decreases, increasing the measurement uncertainty, requiring multi-laser approaches to be employed [49, 50].

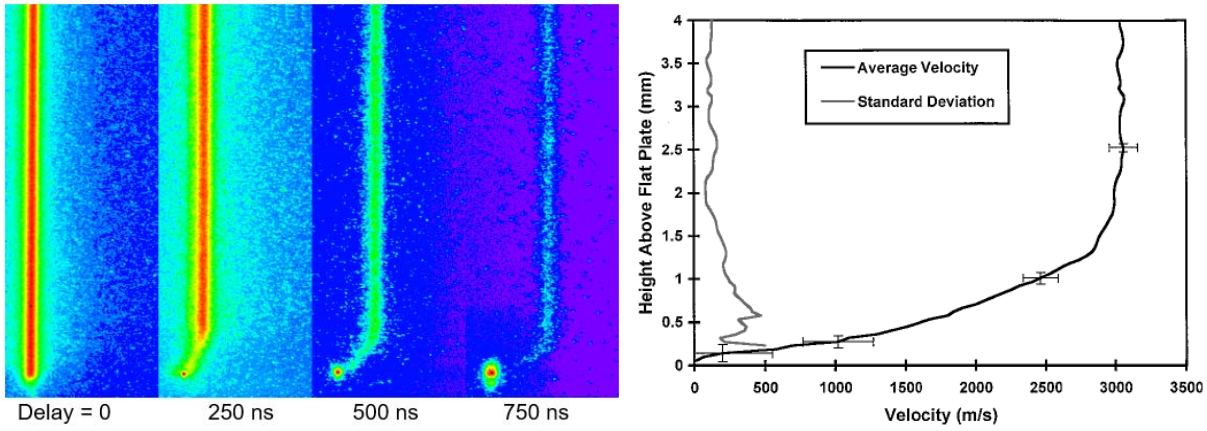

Figure 7. Instantaneous NO MTV raw images obtained of a laminar boundary layer on a flat plate in a free piston shock tunnel at different delays as indicated (left) and a detail of the measured velocity profile and the RMS velocity (right) [31].

2.3. Femtosecond Laser Excitation Tagging (FLEET)

Several measurement techniques taking advantage of high-powered femtosecond and picosecond laser excitation have been developed for unseeded air. The first of these is known as femtosecond laser electronic excitation and tagging (FLEET) [10]. Related techniques that use different excitation wavelengths [51] and different pulse durations [52] have also been demonstrated with each technique having its relative merits. All these approaches have in common the following: (i) they don't require additional gases (or particles) to be seeded, (ii) they use multi-photon excitation to slightly ionize and dissociate nitrogen gas, and (iii) slow recombination of the dissociated

nitrogen species creates long-lived emission that last several microseconds. These long delays allow detection of the tagged molecules at one or more delays. Multiple images are commonly acquired after a single laser pulse allowing velocity, acceleration and particle paths to be measured [40]. Furthermore, additional components of velocity can be measured using additional camera views [40]. However, all of these techniques are nonlinear and require high laser powers which can cause several limitations. Wind tunnel models or windows can be damaged by high laser powers. Furthermore, some variations of the FLEET method can increase the gas temperature significantly. Finally, there is often not enough laser energy to excite many lines in the flow (in comparison to Fig. 5), which limits the number of lines (1 component velocity profiles) or grid crossing points (2 component velocity pointwise measurements) that can be measured. Below, some examples of FLEET and related techniques are discussed and illustrated. While the bulk of FLEET and related techniques have been performed in pure N_2 and air, measurements have also been performed in mixtures of gases. These include nitrogen mixed with argon, helium, carbon dioxide, and oxygen with signal enhancements coming with argon and helium [53-55]. Mixtures of trace concentrations of air with mostly R-134a have been studied since wind tunnels designed to study fluid-structure interaction sometimes use heavy R-134a as the test fluid and this gas is commonly contaminated by air [56].

FLEET performed at 800 nm uses the fundamental output of commercially available titanium sapphire regeneratively-amplified femtosecond lasers, which typically operate with about 100 fs duration pulse at repetition rate of 1-10 kHz with the higher speed models having lower per pulse energy. Energies per pulse at 1 kHz are typically in the range of a 2 to 7 mJ/pulse in currently available commercial models. Depending on the experimental configuration, 800-nm FLEET is typically performed with ~1 mJ/pulse to provide adequate signal to noise while reducing perturbation to the flow and also reducing white-light generation in the optical path.

The first FLEET demonstration was by Michael et al. [10] at Princeton University and is shown in Fig. 8. The 150 fs duration, 1.2 mJ/pulse laser is focused with a 500 mm focal length spherical lens to a beam waste of 30 microns and passed through a 1 mm diameter jet of dry air supplied with 30 psig. The laser passes through the jet perpendicular to the jet's streamwise axis and a camera is oriented normal to the plane of the laser and the jet. The intensified CCD camera uses a 1 μs gate to image the fluorescence delayed 2 μs after the laser excitation. By comparing these delayed images to those acquired at zero delay, instantaneous velocity profiles are measured. Figure 8 also shows resulting averaged velocity profiles.

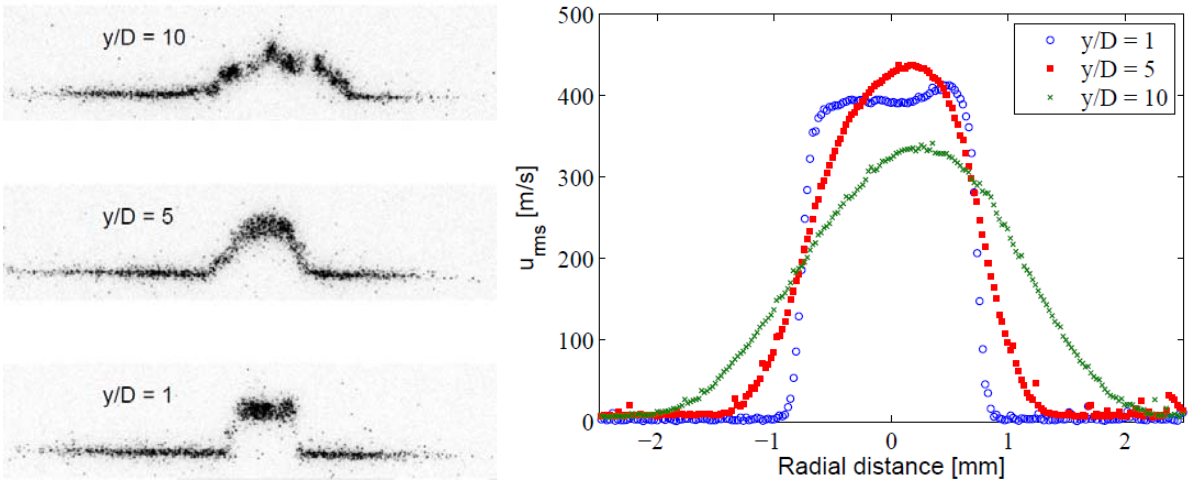

Figure 8 Raw single-shot FLEET signals (left) in a high-speed, dry air jet flow expanded to atmospheric pressure (left) and resulting mean velocity profiles (right) obtained using a 2 µs delay [10].

A subsequent study at Princeton showed that the FLEET technique produced signal intensities nearly an order of magnitude higher in pure N_2 flows than air with comparable lifetimes [57]. Thus, it was anticipated that the technique would work especially well in pure-N_2 wind tunnels such as The Arnold Engineering Development Complex's (AEDC's) Tunnel 9 and NASA Langley's Transonic Cryogenic Tunnels. Even more recently, the technique has been demonstrated in Sandia National Laboratories Mach 8 nitrogen tunnel [58] and Purdue University's Mach 6 quiet tunnel which also operates on N_2.

A setup similar to Fig. 8 was used to measure the freestream flow in the AEDC Tunnel 9 facility in Maryland [59]. An intensified CMOS camera was used to image the tagged molecules several times after each laser excitation pulse from the 800-nm femtosecond laser. The velocity is determined from the spacing of the lines, considering the uneven gate durations and delays used to keep the signal intensities comparable in the delayed images. Measurement uncertainties of ~ 0.5% of the measured velocities were reported and good agreement with the velocity predicted by a computational code was shown (see bottom row in the Figure 9).

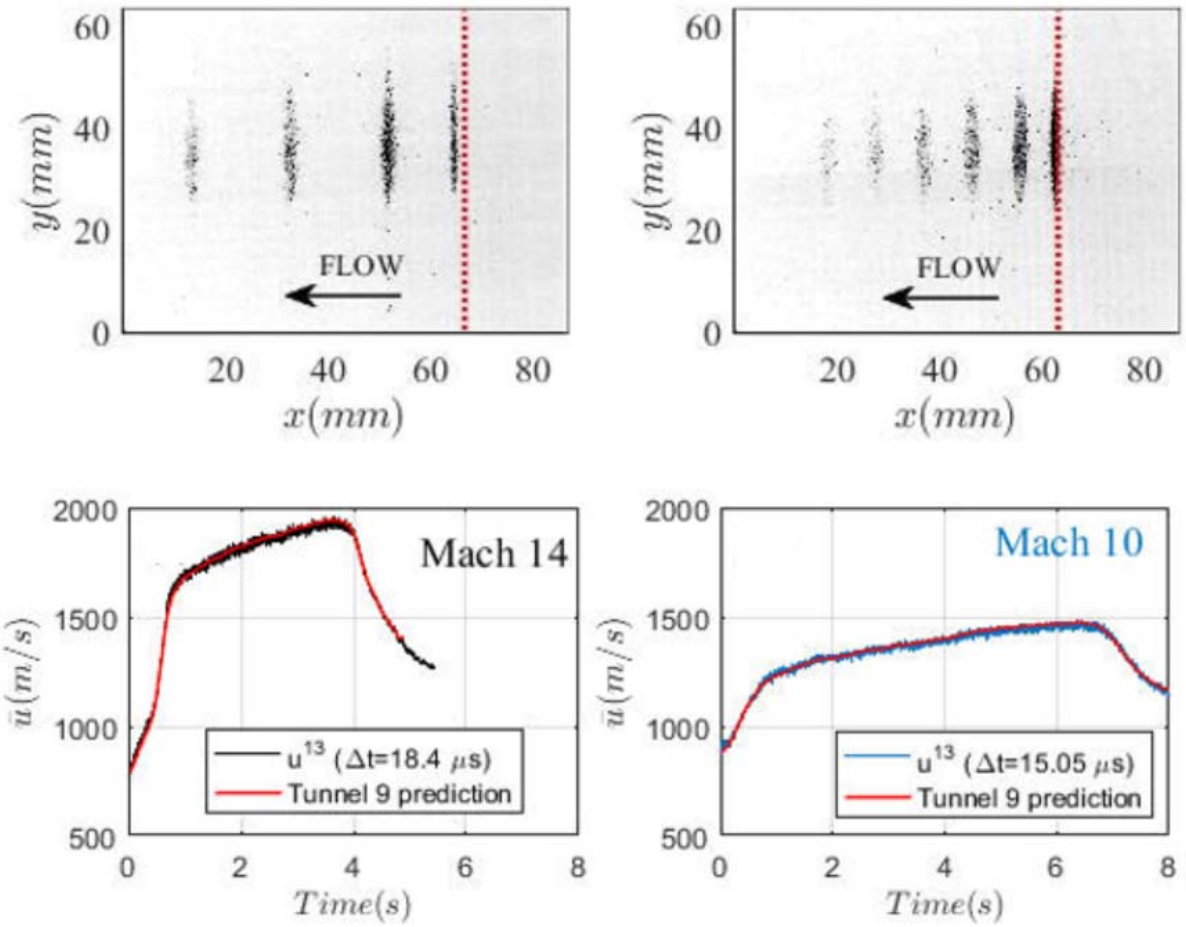

Figure 9. Raw (top row) and processed (bottom row) single-shot FLEET velocimetry data acquired in the AEDC Tunnel 9 facility freestream at Mach 14 (left column) and Mach 10 (right column) [59].

In the NASA Langley Research Center 0.3-m Transonic Cryogenic Tunnel (TCT) operating in pure N_2, the FLEET method was used to probe the flow around a wing [41]. A so-called "quasi-boresight" configuration was used where the laser and the camera look through the same window, nearly along the same axis, so the FLEET emission appears as a point allowing two components of velocity to be measured with a single camera. A 70 fs duration, 1 mJ/pulse laser was focused into the flow using a 300 mm focal length lens. The resulting emission was imaged by an intensified high-speed camera in a sequence of four exposures over 25 microseconds. In Figure 10, flow is left to right over a wing mounted to the opposite tunnel wall. The laser passes nearly parallel to the surface of the wing exciting a spot which is then imaged as it convects around the wing. The laser was translated to different positions in the camera's field of view by using motorized periscopes. The resulting velocity profiles show subsonic, steady, attached flow on the bottom of the wing and supersonic, more unsteady, attached flow on the upper surface of the wing until reaching mid-chord. Downstream of this chordwise position the flow is observed to become highly unsteady (as indicated by the lower graph) and is observed to separate. Downstream of the wing the expected velocity deficit is observed in the mean. As the flow continues further downstream the velocity gradients are smoothed out by turbulent diffusion.

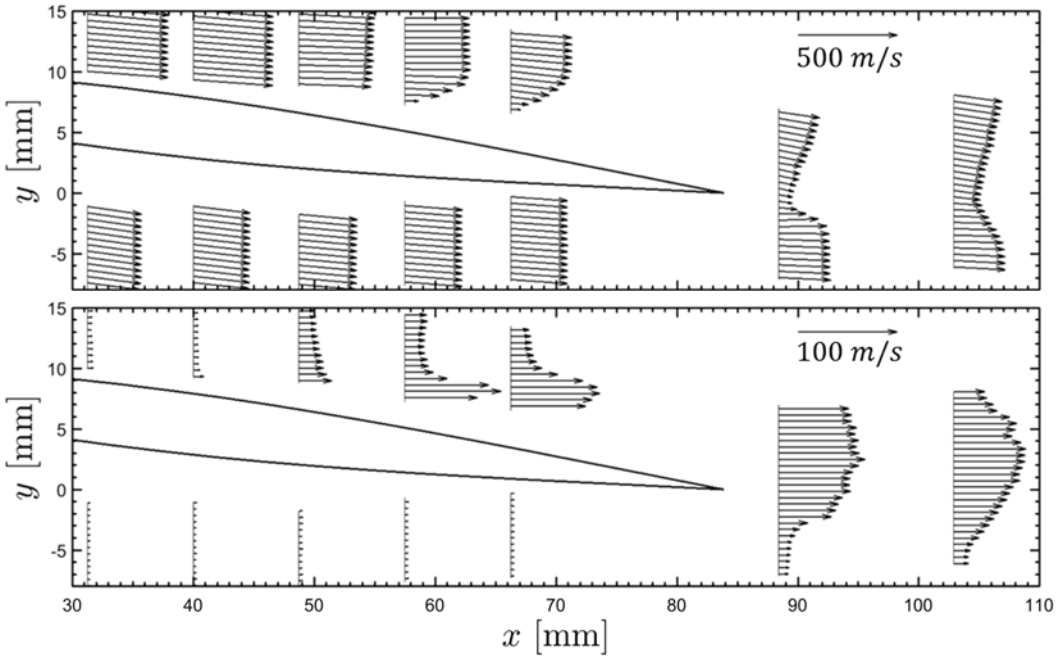

Figure 10. Two-component mean (top) and fluctuating (bottom) FLEET velocity measurements near a wingat a 7 degree angle of attack at Mach 0.85 [41]. Fluctuation magnitudes were computed from $(\langle u_x' \rangle^2 + \langle u_y' \rangle^2)^{1/2}$.

The series of FLEET experiments in this same facility [42, 43] showed that the technique could operate over the full operational range of the facility (down to 100 K and up to 400 kPa), that the FLEET signal is proportional to the gas density, and the lifetime is inversely proportional to density (described in more detail in section 4.1), at least between 1 and 7 kg/m^3. However, the FLEET signal intensity cannot be used to measure gas density from either signal intensity or lifetime in flows containing shear because the signal intensity and lifetime depend strongly on the local fluid environment in addition to the static conditions [43].

More recently, the 800-nm FLEET technique has been demonstrated in NASA Langley's National Transonic Facility (NTF) which has an 8 foot (2.43 m) square test section [60]. Density measurements based on Rayleigh scattering have also been demonstrated with the same setup in the same facility, potentially allowing mass flow measurements (ρuA, where ρ is the density, u is the velocity and A is the area) which would be especially useful in propulsion applications sometimes performed in the NTF.

Other variations of FLEET have been demonstrated using different wavelengths and different pulse durations. Using harmonics of the 800-nm light shows potential to provide comparable signal intensities while using less overall energy per pulse which is potentially less damaging to test articles and facility windows and less perturbative to the flow. For example, FLEET has been performed by doubling the 800-nm light to 400 nm, achieving higher signal-to-noise ratio images [61]. Similarly the 267-nm, frequency-tripled output of an 800-nm laser has been use to write narrower lines in the flow (on the order 150 microns wide using a 300-mm focal length lens), providing higher spatial resolution, allowing the Taylor microscale to be measured [54]. The

STARFLEET technique [51] which uses 202.25-nm light obtained by quadrupling an 809-nm femtosecond laser to resonantly excite N_2. This method uses just ~50 μJ of energy per pulse, resulting in only a 10 K increase in temperature of the flow compared to an ~230 K increase from 800-nm FLEET in one direct comparison [51]. STARFLEET has also been demonstrated in the Langley 0.3-m TCT to study the wake flow behind a cylinder [62]. Finally, laser electronic excitation and tagging has been performed with a picosecond laser (PLEET) at 1064 nm. The advantage of this method is that the picosecond laser could be operated at 10-100 kHz to obtain measurements at 10-100x faster than prior 1 kHz FLEET [52]. A 100 ps laser was also successfully demonstrated in the Langley 0.3 meter TCT although these measurements were less precise compared to FLEET measurements at the same conditions [63]. Very recently, a new MHz femtosecond laser technology has been developed and FLEET has been demonstrated at 1 MHz in a jet flow, showing potential to provide time resolved velocimetry even in hypervelocity flows [64].

3. Multiple-Laser Methods

3.1 Photodissociation or Photofragmentation Tagging

In photodissociation or photofragmentation tagging, the laser dissociates molecules in the gas to form a line or grid of stable tag molecules. In some methods, the tag forms immediately from photofragmentation. In HTV, the OH tag is a direct photo-fragment of H_2O [1]. Photo-fragmentation of tert-butyl nitrate $(CH_3)_3CONO$ produces NO directly [38]. In other methods, the tag forms by chemical reactions that dictate the formation time. In OTV, the ozone tag results from photodissociation of O_2 into O atoms that combine with O_2 to form O_3 [15]. In APART, the 193-nm laser photo-ionizes N_2 to N_2^+ leading to the formation of N atoms that subsequently react with O_2 to form NO [65]. In imidogen tagging velocimetry, a 193-nm laser dissociates N_2 into N_2^+ leading to N atoms that subsequently react with H_2O or H_2 to form the NH tag [21]. In N_2O photodissociation tagging, the 193-nm laser dissociates N_2O into N_2 + O (^{1}D) and the O (^{1}D) reacts with N_2O to form NO [36, 37] .

3.1.1 Hydroxyl Tagging Velocimetry

In hydroxyl tagging velocimetry [1], a 193-nm laser dissociates water vapor in the gas to form a tag line of OH by a one-photon process: $H_2O + h\nu_{193nm} \rightarrow OH + H$. The tag line is displaced by the gas flow and then the OH line is excited with a second laser to image the displaced line. An example is shown in Fig. 11 where the ArF laser beam is split into multiple beams to form a 7x7 grid in a flowfield. The doubled output from an Nd:YAG pumped dye laser at 308 nm excites OH fluorescence that is imaged by an ICCD camera. Alternatively, a XeFl excimer laser at 308 nm can directly read the displaced OH grid.

The HTV system can be applied to non-reacting, moist, high-speed air flows (Fig. 1) and is applied to measure the hot products over a Hencken burner flame in Fig. 12 [66]. The velocity measurements are made downstream in the post-flame zone of nearly adiabatic equilibrium products. Since HTV is a single-photon excitation process, a large area of the post flame zone can be imaged (25 mm x 40 mm) showing the uniformity of the flow over the Hencken burner.

The lifetime of the OH tag in air flows is ~20 μs [67] and in lean flames is ~100 μs [66] allowing the method to be used over low-speed flows and high-speed flows. In low-speed flows (1-3 m/s), measurement uncertainty of 0.1 m/s at a 68% confidence level has been demonstrated [68]. HTV has been applied to measure high-speed flows such as a Mach 2 air flow over a cavity [2, 69] or strut/cavity [70], gas turbine exhausts [71], shock tube flows [72], dual-mode scramjet combustor [73] and rocket exhausts [74].

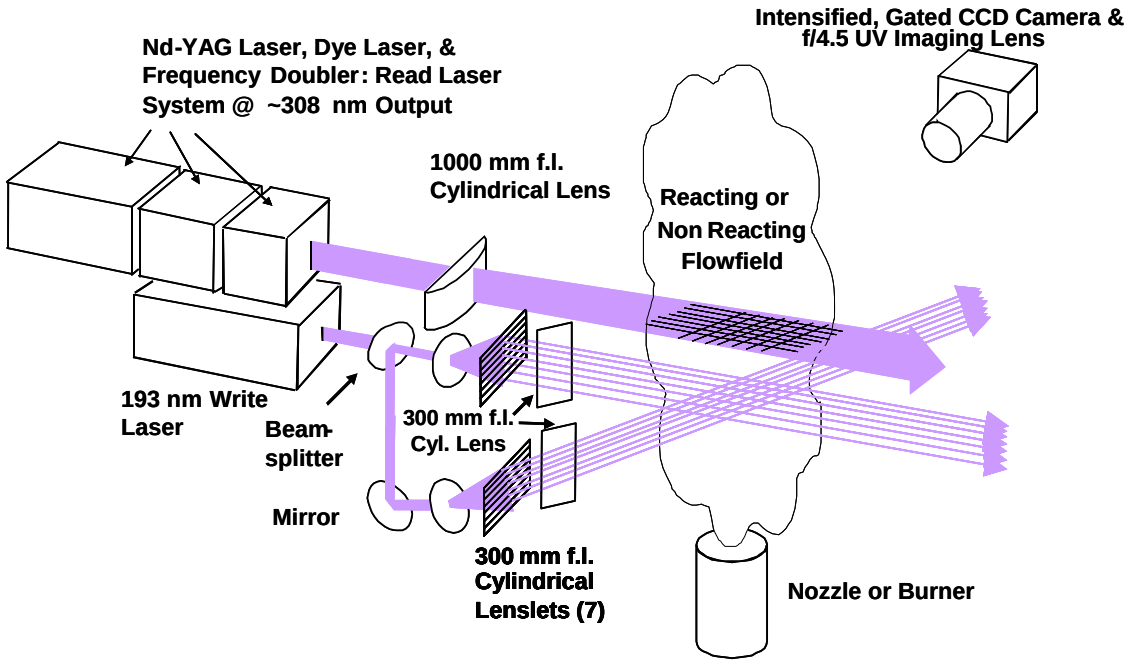

Fig. 11. Hydroxyl Tagging Velocimetry (HTV) schematic [66].

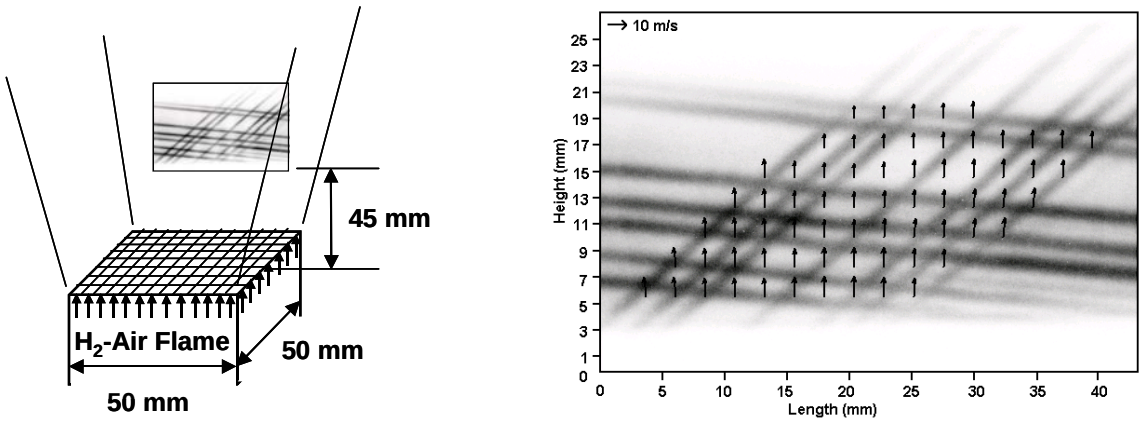

Fig. 12. Measurement of the velocity flowfield over a Hencken burner flame (H_2/air, ϕ=0.39, T=1400 K) The grid is recorded at 0 μs and 50 μs (displaced image on the right) [66].

3.1.2 Ozone Tagging Velocimetry (OTV)

In ozone tagging velocimetry (OTV) developed by Pitz et al. [15], a 193-nm ArF excimer laser creates a line of ozone in oxygen-containing flows and the displaced tag line is imaged with a 248-nm KrF excimer laser. The optical setup for the OTV measurements is shown in Fig. 13 for a two-line configuration over an air jet. The 193-nm ArF laser forms a tag line of O atoms in air and the O atoms chemically react in ~20 μs in room air to form ozone:

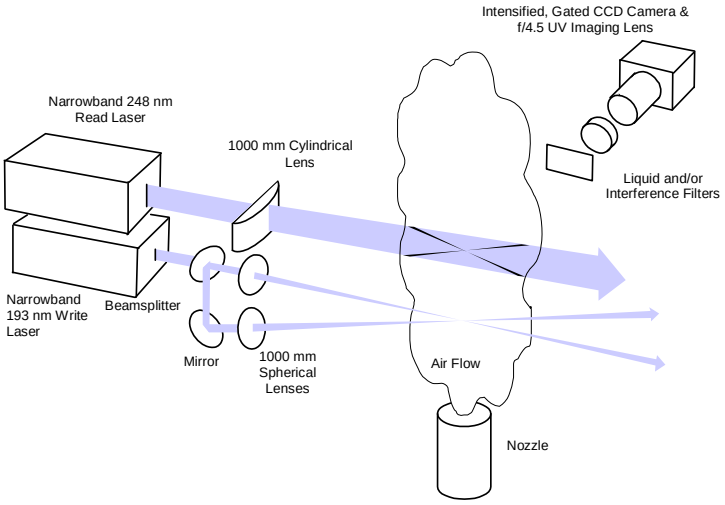

$$O_2 + h\nu_{193nm} \rightarrow O + O \qquad (1)$$

$$O + O_2 + M \rightarrow O_3 + M \qquad (2)$$

Fig. 13. Ozone tagging velocimetry (OTV) system using two excimer lasers [17].

To "read" the displaced line, the ozone is photo-dissociated by a sheet of 248-nm laser and the same sheet of 248-nm light from a KrF excimer laser excites O_2 fluorescence in the Schumann-Runge band [15-17]:

$$O_3 + h\nu_{\lambda=248\ nm} \rightarrow O\ (^3P) + O_2\ (X^3\Sigma^-_g,\ v''>0) \qquad (3)$$

$$O_2\ (X^3\Sigma^-_g,\ v''=6,7) + h\nu_{\lambda=248\ nm} \rightarrow O_2\ (B^3\Sigma^-_u, v'=0,2) \rightarrow O_2\ (X^3\Sigma^-_g) + h\nu \qquad (4)$$

Multi-line (3x3 grid) OTV measurements were made at 25 diameters downstream in a 12.5 mm diameter air jet (20 SLPM of air, ~2.5 m/s at exit) at atmospheric pressure and room temperature and the displaced, un-displaced, and velocity field images are shown in Fig. 14 [16]. The OTV technique cannot be used above 600 K due to the thermal decomposition of ozone (see Fig. 21,

right) [17]. Ozone is depleted by the presence of NO in the gas (Fig 21, left) [15] and for low temperature studies, ozone condenses to a liquid at a temperature of 161 K.

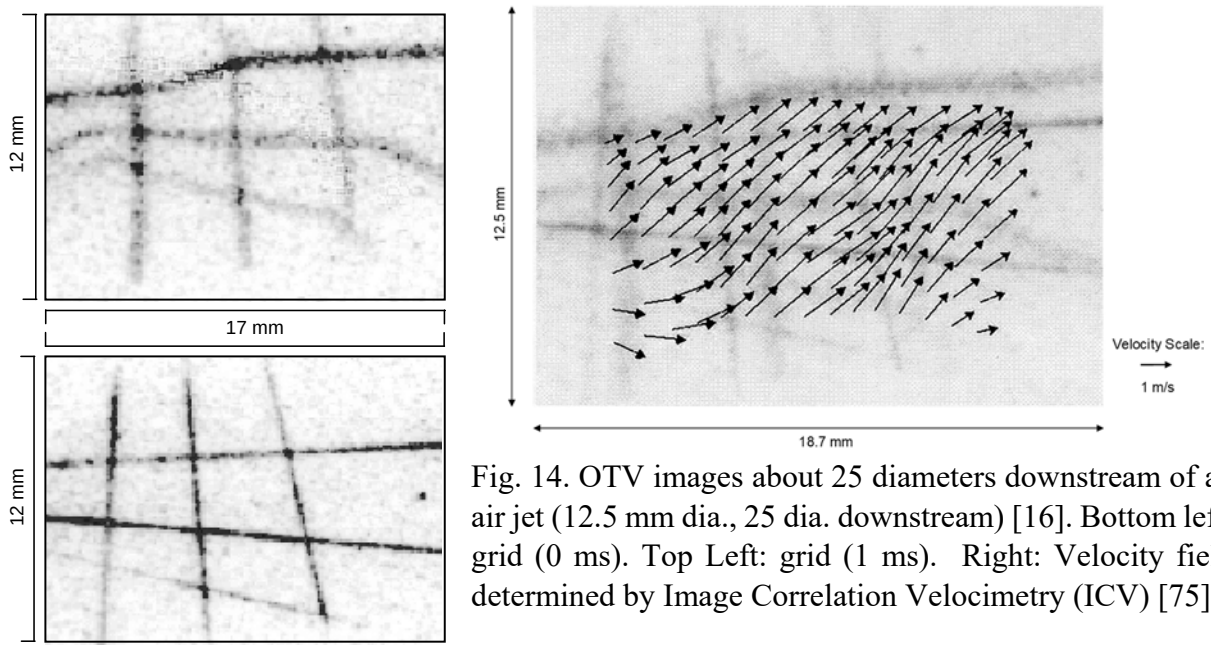

Fig. 14. OTV images about 25 diameters downstream of an air jet (12.5 mm dia., 25 dia. downstream) [16]. Bottom left: grid (0 ms). Top Left: grid (1 ms). Right: Velocity field determined by Image Correlation Velocimetry (ICV) [75].

3.2 Vibrationally excited tags

Vibrational excitation can distinguish the molecular tag from the other molecules in the gas. In RELIEF described below, the vibrational ground state $O_{2\ v=0}$ is excited to $O_{2\ v=1}$ by stimulated Raman scattering along collinear 532-nm and 580-nm laser beams where v is the vibrational quantum number. In other MTV methods, photo-dissociation of larger molecules produces vibrationally excited products. In vibrationally excited NO monitoring (VENOM), $NO_{v=1}$ is produced [34] and in vibrationally excited hydroxyl tagging velocimetry (VE-HTV), $OH_{v=1}$ is produced [14]. These excited state tags can be distinguished from background $NO_{v=0}$ and $OH_{v=0}$ in the gas through selective laser excitation of the v=1 states only. A feature of vibrationally excited tagging is that the rate of equilibration of vibrationally excited states is relatively slow so the tag lifetime is long compared to the time scales of the flow.

3.2.1 Raman excitation plus laser-induced electronic fluorescence (RELIEF)

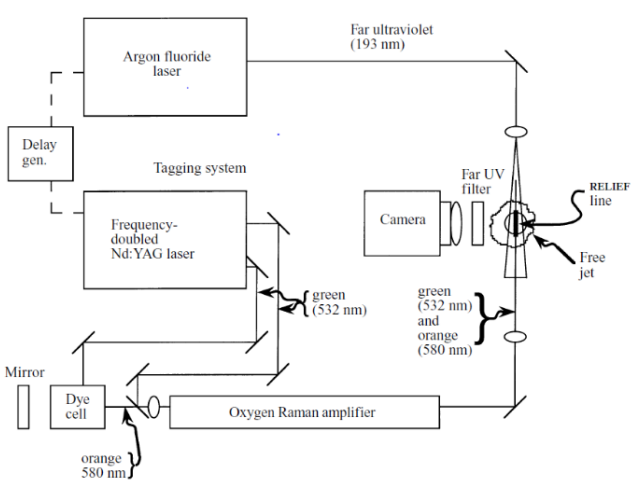

Raman excitation plus laser-induced electronic fluorescence (RELIEF) is an early multi-laser MTV method developed by Miles et al. [18] that uses stimulated Raman scattering to vibrationally excite O_2 from v=0 to v=1 where v is the vibrational quantum number. The $O_{2\ v=1}$ molecules have a long lifetime (~1 ms) in room temperature nitrogen or dry air and can be imaged with an ArF excimer laser. A schematic of the optical setup is seen in Fig. 15 [20].

Fig. 15. Schematic of the RELIEF system [20].

A 532-nm beam is focused into a Raman cell of high-pressure O_2 gas. A dye cell generating 580-nm light is used to help seed the Raman cell to generate a 580-nm beam. The combined 532-nm and 580-nm beams are focused into a free jet containing oxygen and cause vibrationally excited $O_{2\ v=1}$ to form along the line by stimulated Raman scattering. The tagged lines are illuminated by LIF from a 193-nm ArF excimer laser (Fig. 16). The non-linear stimulated Raman process can form 100 µm diameter lines to interrogate scales as small at 25 µm in a near room temperature turbulent air jet flowfield [20].

The RELIEF method is limited to gas temperatures below ~700 K [76]. Higher temperatures will lead to equilibrium levels of $O_{2\ v=1}$ that obscure (reduce the contrast of) the RELIEF lines. Also water vapor in humid air (50% humidity, 1% mole fraction) reduces the $O_{2\ v=1}$ tag lifetime to ~20 µs [76].

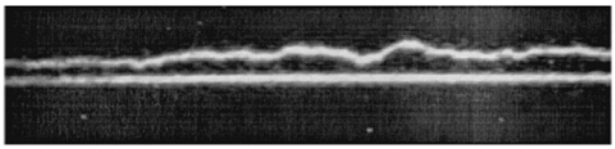

Fig. 16. RELIEF tag lines (100 µm dia., 1 cm long) written in a turbulent jet [20].

3.2.2 Vibrationally excited NO monitoring (VENOM)

In the VENOM method, and the gas flow is seeded with NO_2 that is photo-dissociated by a 355-nm laser beam into NO producing ground vibrational state $NO_{v=0}$ and $NO_{v=1}$ in a 60/40 ratio [34, 44]:

$$NO_2 + hv_{\lambda=355nm} \rightarrow O + NO_{v=0} \quad (5)$$

$$NO_2 + hv_{\lambda=355nm} \rightarrow O + NO_{v=1} \quad (6)$$

In VENOM, the $NO_{v=1}$ tag is imaged with the advantage that it can be seen even in a background containing $NO_{v=0}$. In Fig. 17, the VENOM method is applied to the high-speed flow of an axisymmetric underexpanded free jet [34]. In Fig. 17 (left), the 355-nm laser forms a single tag

line in the jet flowfield that is imaged by planar ~225-nm laser sheet. In Fig. 17 (center), the images of the NO tag lines are shown for both $NO_{v=0}$ and $NO_{v=1}$. The $NO_{v=1}$ tag lifetime is ~5 µs [34]. Using the vibrationally excited tag, $NO_{v=1}$, the streamwise velocity flowfield is determined in Fig. 17 (right). The method has also been demonstrated to measure two components of velocity [44] and simultaneous velocity/temperature in underexpanded free jets [77]. More recently a version of the VENOM technique has been developed using NO seeding instead of the more difficult to use NO_2 [50].

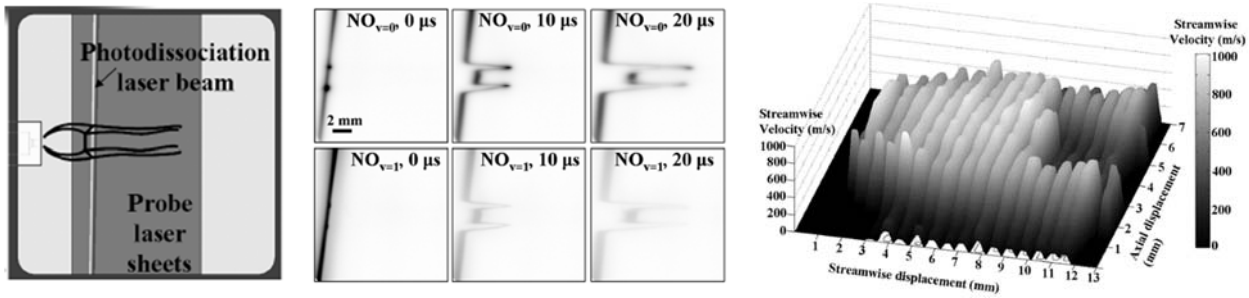

Fig. 17. Molecular tagging with vibrationally excited NO monitoring (VENOM) [34]. Left: 355-nm photodissociation laser beam and probe laser sheet in the underexpanded free jet (1 mm dia. throat, 455 torr stagnation pressure, 5 torr ambient pressure). Center: NO tag line images for $NO_{v=0}$ and $NO_{v=1}$ at various time delays. Right: Streamwise velocity field of the jet from the $NO_{v=1}$ tag.

3.2.3 Vibrationally excited hydroxyl tagging velocimetry (VE-HTV)

In flames, the OH background is high and can obscure the HTV grid (Fig. 38). The background OH in the flame is predominately in the vibrational ground state, $OH_{v=0}$ and measuring an $OH_{v=1}$ tag can reduce this background. In vibrationally excited HTV, a tag line of vibrationally excited $OH_{v=1}$ forms by two-photon 248-nm photodissociation of H_2O from a KrF excimer laser beam [14]:

$$H_2O + hv_{\lambda=2x248nm} \rightarrow H \ + \ OH_{v=1} \qquad (7)$$

The $OH_{v=1}$ tag is imaged with a 347-nm laser sheet to excite the $A^2\Sigma^+$ (v′=0) ← $X^2\Pi$ (v″=1) band of OH. In Fig. 18, the VE-HTV $OH_{v=1}$ lines are shown from the post-flame zone of a H_2/air Hencken burner flame at lean (ϕ=0.75, 2103 K), near stoichiometric (ϕ=0.95, 2355 K), and rich (ϕ=1.51, 2245 K) conditions. The VE-HTV lines are clearly seen above the $OH_{v=1}$ background that is also illuminated by the 347-nm laser sheet.

The measured intensity of the VE-HTV signal vs. equivalence ratio in the Hencken burner flame is shown in Fig. 19 (left). Also shown are the calculated adiabatic equilibrium values of temperature and species number density. The VE-HTV signal peaks at stoichiometric conditions and is lower at lean and rich conditions. At stoichiometric conditions, the $OH_{v=1}$ number density is about 10% of the total OH giving rise to the background seen in Fig. 18.

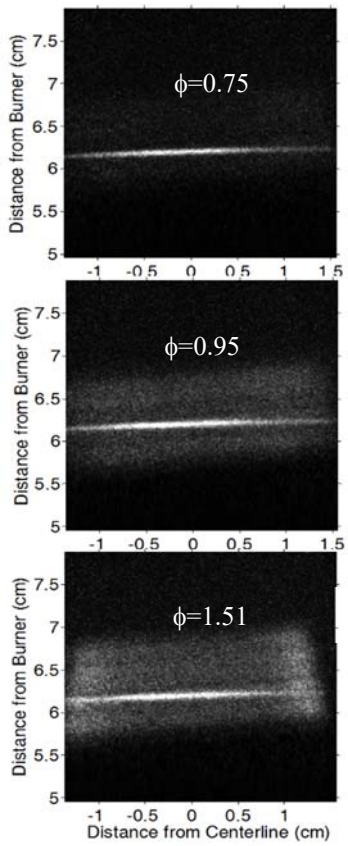

Fig. 18. Vibrationally excited hydroxyl tagging velocimetry (VE-HTV) images in the adiabatic post-flame zone of a H_2/air Hencken burner flame at lean (ϕ=0.75, 2103 K), near stoichiometric (ϕ=0.95, 2355 K) and rich (ϕ=1.51, 2245 K) conditions. The time delay is 10 μs [78].

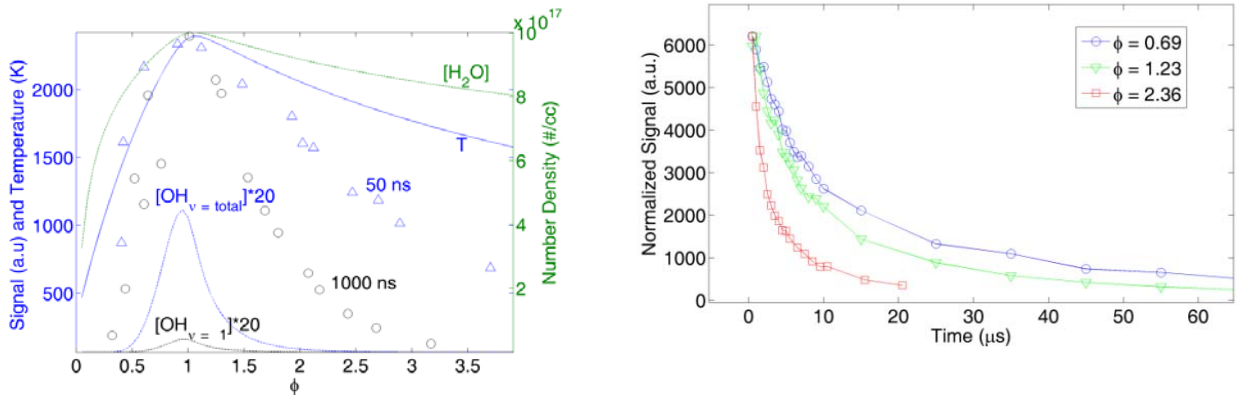

Fig. 19. Measurements of $OH_{v=1}$ tag signal in the adiabatic post-flame zone of a H_2-air Hencken burner [14]. Left: $OH_{v=1}$ signal intensity vs. equivalence ratio (ϕ) at two different time delays (Δ 50 ns, o 1000 ns). The adiabatic equilibrium values of temperature and species number densities (#/cm^3) are shown. Right: The measured $OH_{v=1}$ signal vs. time for various ϕ's.

As shown in Fig. 19 (right), the measured tag lifetime of $OH_{v=1}$ is longest (~60 μs) in lean and stoichiometric flames and shortest (~20 μs) in rich flames where the OH is consumed by excess H_2 fuel.

4. Tagging Issues: Lifetime, Diffusion, and Heating

4.1 Tag Lifetime

For molecular tagging velocimetry, the tag lifetime must be sufficient to record the displaced line. For single-laser methods, the displaced line is imaged with light emission from tagged atoms/molecules whose excited states can be affected by collisional quenching and chemical reaction. In multiple-laser methods, the displaced tagged molecules are read by an imaging laser that excites a particular excited state or chemical state that must be retained in the displaced line in the presence of chemical reaction. Thus, it is important that the MTV tag lifetime be sufficient for the desired application that has a characteristic velocity, pressure, temperature, and gas composition.

Lifetime is especially important – and potentially limiting – in single-laser methods. For example, as detailed in section 2.2 on *Nitric oxide (NO) fluorescence tagging velocimetry*, the fluorescence lifetime of NO in the absence of collisions is only 200 ns which limits this technique's application to very high-speed flows (greater than a few hundred m/s) so that the tagged molecules can move appreciably between excitation and acquisition. In addition, the short lifetime limits single-laser NO MTV to either low density or non-quenching (e.g. mostly nitrogen or helium) flows. In air flows, at the gas density increases, the NO lifetime decreases proportionally resulting in such short lifetimes that the technique is not viable, even for high-speed flows, requiring the use of an alternate two-laser MTV measurement technique [35, 79].

The FLEET method is a single-laser method that exhibits lifetimes much longer (about 10 μs) than NO PLIF MTV. FLEET has been shown by various authors to have long lifetimes over a wide range of conditions. Miles's group at Princeton were the first to observe the long (microseconds) FLEET lifetimes in both air and N_2 in a room temperature gas cell over a wide range of sub-atmospheric pressures [80, 81]. DeLuca et al. [82] found that FLEET lifetime in post flame zone of a methane-air Hencken burner was 0.27-0.63 μs which is shorter than their values in laboratory air (0.85 μs) and nitrogen (2.2 μs). Sub-microsecond lifetimes were sufficient to measure velocity in the exhaust of a high-speed pulsed detonator [82]. Burns et al. [83] measured and reported the lifetimes of FLEET as a function of both temperature and pressure in the range of 100-280 K and 100-400 kPa in nitrogen. In this study [83], the authors found the lifetime was best fit by a tri-exponential. Both 1/e and $1/e^2$ lifetimes were measured and plotted versus temperature, pressure and density as shown in Figure 20. The lifetimes were found to correlate well with the gas density (at least over this range of conditions) and fit coefficients were provided. Subsequently, Peters et al. [84] have modeled the FLEET lifetime from first principles using a zero dimensional model.

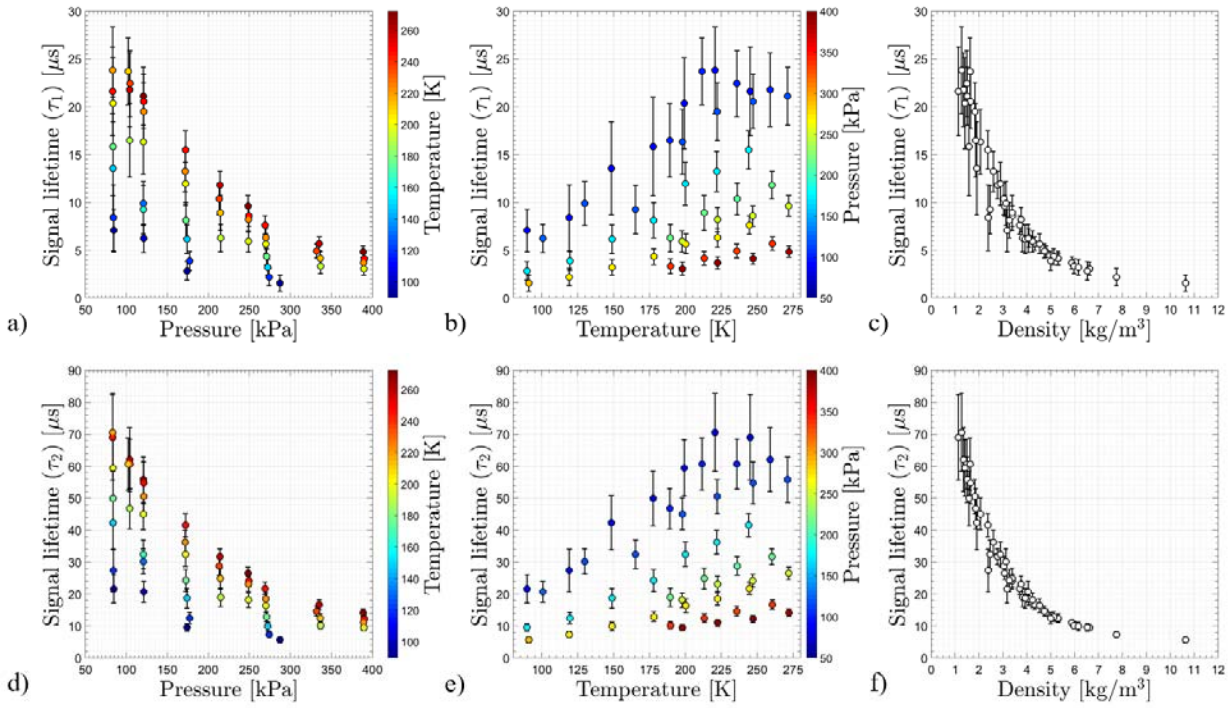

Figure 20. FLEET $\tau_1 = 1/e$ and $\tau_2 = 1/e^2$ lifetimes in compared with pressure, temperature and density over a range of temperatures below room temperature and pressures above atmospheric pressure nitrogen in a transonic cryogenic wind tunnel. From Burns et al. [83].

For ozone tagging velocimetry (OTV), a multi-laser technique, the ozone tag is chemically created from dissociation of O_2 by the 193-nm ArF laser. An example of predictions of ozone tag formation is shown in Fig. 21 [15, 17] using the SENKIN code of CHEMKIN [85] and the chemical kinetic mechanism from Richard Yetter [86]. In room temperature air (Fig. 21 left), the ozone tag forms in ~20 µsand is stable beyond 1 s [15]. Ozone is depleted by the presence of NO contamination. The 1% O_2 dissociation by the laser leads to a temperature increase of ~30 K. Predictions at higher temperature in room air are shown in Fig. 21 (right) [17]. At a higher temperature of 600 K, ozone decomposes and disappears after ~100 ms.

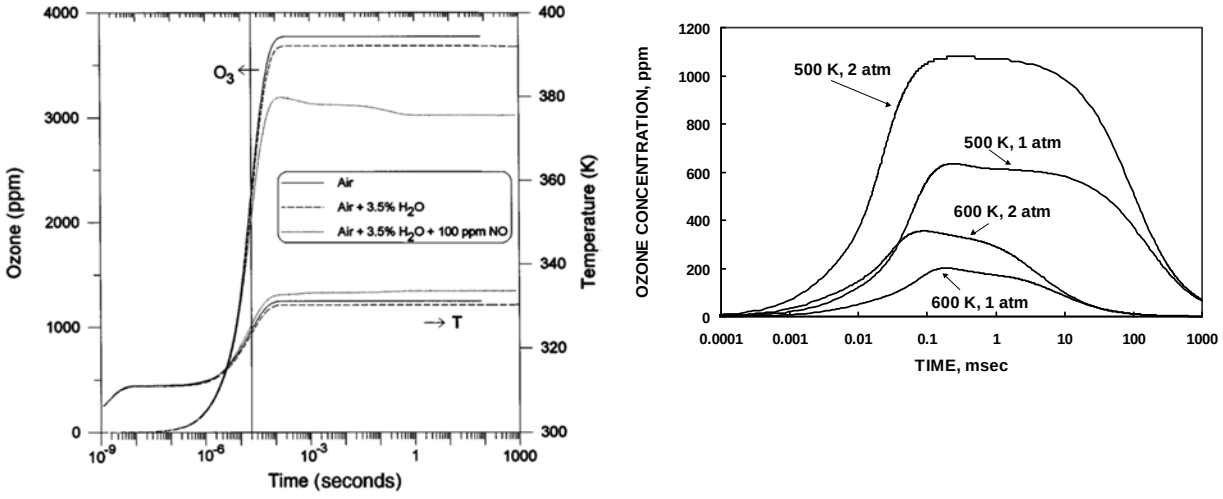

Fig. 21. Prediction of ozone formation assuming 1% dissociation of O_2 by the ArF laser. Left: room air at 1 atm. (dry, moist, with NO) [15]; Right: Dry air at higher pressures and temperatures [17].

In hydroxyl tagging velocimetry (HTV), an OH tag is produced that has a short lifetime in room air (~20 μs) [67] and longer lifetime in high temperature lean flames (~100 μs) [1]. The predicted lifetime in room temperature air is shown in Fig. 22 (left) using the SENKIN code and a chemical kinetic mechanism from Yetter [67]. Including the O atoms from 193-nm O_2 photo-dissociation gives better agreement between prediction and measurement. As the air temperature is increased, the predicted OH tag lifetime increases to 100 μs at 1500 K.

For high temperature flames, the OH lifetime is long (~100 μs). Under lean conditions (ϕ=0.43 H_2/air), H atoms from photo-dissociated H_2O form additional OH to extend the tag lifetime (see Fig. 22 (right). The OH formation is calculated with the SENKIN code and the GRI-Mech 2.11 chemical kinetic mechanism [1]. Under rich conditions (ϕ=4.36), the OH is rapidly oxidized by excess fuel leading to short lifetimes (0.1 μs).

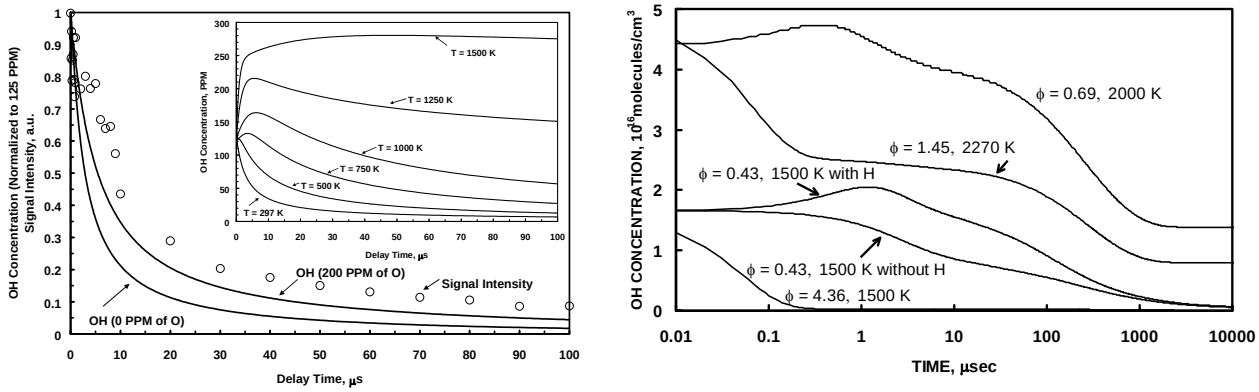

Fig. 22. Left: OH lifetime in room air (40% relative humidity), predictions assume 1% H_2O dissociation [67]. Right: OH lifetime predictions in H_2/air adiabatic equilibrium mixtures using temperature-dependent H_2O 193-nm absorption cross-sections [1].

In the N_2O MTV method [36], the flow is seeded with a few percent N_2O. Unlike NO_2 photodissociation that directly forms the NO tag as a photo-fragment, N_2O photodissociation produces the NO tag by a two-step chemical process. As seen in Fig. 23, the NO tag forms very quickly (~10 ns in room air) by ArF excimer laser dissociation of N_2O into $O(^1D)$ that subsequently reacts with the remaining N_2O:

$$N_2O + hv_{\lambda=193nm} \rightarrow N_2 + O(^1D) \quad (8)$$

$$N_2O + O(^1D) \rightarrow 2NO \quad (9)$$

For 25% N_2O photodissociation, the measured and calculated formation of NO is shown in Fig. 23 for room air conditions. The NO formation rate is calculated with the SENKIN code [85] and an atmospheric chemical kinetic mechanism [36]. The formation rate of NO is controlled by reaction (9) and is ~10 ns for a 4% N_2O-air mixture at 298K and 1 atm. Once formed, the NO tag is very stable in room air. Andre and coworkers [37] exploited the similarly long lifetimes of photodissociated NO from N_2O, helium and nitrogen mixtures to measure velocity in very low speed flows with velocities on the order of 1 m/s with a measurement precision better than 0.01 m/s.

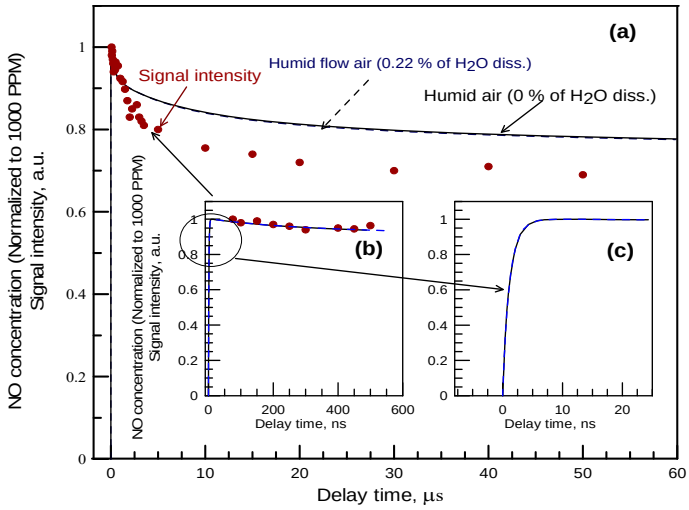

Fig. 23. Measured and calculated NO formation time for N_2O MTV in a 4% N_2O-air mixture at 297 K and 1 atm. NO formation time is consistent with reaction (9) controlling rate constant of $k_9 = 7.2 \times 10^{-11}$ cm^3/ molecule under standard conditions. Time of formation of 63% of the steady-state NO concentration (at STP) is $1/(2\, k_9\, n_{N2O}) \approx$ 10 ns where n_{N2O} is the N_2O number density after dissociation [36].

4.2 Tag Diffusion

The tag molecules will diffuse with time making the tag line more difficult locate due to its greater width and reduced tag molecule density. The tag diffusion width, w, at time delay, Δt, is [87],

$$w = [8 \ln(2)\, \Delta t\, D + w_o^2]^{1/2} \quad (10)$$

where D is the gas diffusivity and w_o is the initial tag width. Heating of the gas by the laser will increase the tag width beyond that given by Eqn. 10 [88]. For N_2 diffusing into N_2 at room conditions ($D_{N2/N2}$=0.2 cm^2/s), an infinitely thin tag line will grow to 1 mm wide in 9 ms (Eqn. 10). Tag diffusion is most important in low-speed flows where longer delay times are required. N_2O MTV has been applied to low speed flows and diffusion of a 1 mm NO tag line in nitrogen and helium is shown in Fig. 24 [37].

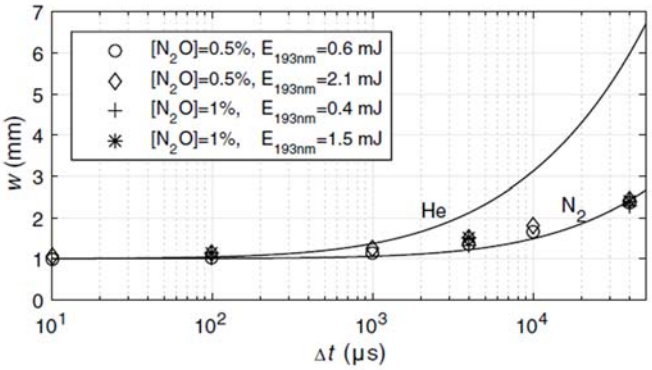

Fig. 24. Diffusion of a 1 mm wide tag line of NO in N_2 and He using N_2O MTV at room conditions (1 atm, 293 K). The NO tag is produced by 193-nm photo-dissociation of N_2O at various energies. Symbols show measured values in N_2 and lines are from Eqn. 10 ($D_{NO/N2}$=0.23 cm^2/s, $D_{NO/He}$=1.58 cm^2/s) [37].

4.3 Tag Heating

Tagging gases with high-powered lasers adds localized heat to the flowfield. This energy addition can have various affects. For example, it could cause the flow to transition from laminar to turbulent, which is sometimes done intentionally in order to study transitional flows [89]. Spectrally resolved emission measurements have shown that the heating can be 100's of Kelvins in some experiments such as FLEET [11, 51]. This heating can have negligible impact on the experiment if the flowfield downstream of the measurement is not a concern. In such cases, the measurements could still be considered less perturbative than rakes and probes that have been used for decades. More importantly, the heat addition can cause the tagged fluid to not follow the flow owing to buoyancy, resulting in erroneous velocity measurements. That is, heated, less dense, buoyant fluid might not follow flow streamlines in a similar but opposite way that heavy particles do not follow the flow.

Limbach and coworkers [88] used Rayleigh scattering to visualize the shock waves emitting from the FLEET focus, as well as to quantify the decrease in density and corresponding increase in temperature at the core of a femtosecond laser tagged region. Temperature increases over 1000 K were observed using less than 1 mJ/pulse in the femtosecond tagging beam with a relatively short 175 mm focal length focusing lens. Burns et al. [63] computed that the buoyance of even a 1000 K local temperature increase would only change the vertical velocity by a fraction of a meter per second (0.04 m/s) over a 250 μs measurement timescale for flow traveling in a straight horizontal line, which is small compared to the 1.2 m/s measurement precision obtained at the conditions of the computation. New-Tolley et al. showed that a 600 K temperature increase had a negligible effect on the measured velocity in a laminar boundary layer but it artificially thickened a computed shear layer flow [90]. These papers provide different, mostly complementary frameworks for determining whether heat addition associated with laser tagging will affect the measured velocities in MTV experiments. It should be noted that none of these analyses addressed the combination of buoyancy and streamline curvature that cause potentially cause significant velocity errors in MTV experiments that involve significant heat addition.

5. Multi-Dimensional Measurement, Grid Formation, 2D Velocity, 3D Velocity

5.1 Grid Formation.

A single tag line (Fig. 17), a two-line cross (Fig. 13), or a 3x3 grid (Fig. 14) can written with lenses and beam splitters. For high-density grids, aluminum slotted plates [24, 91] or aluminum meshes [44, 77] are the easiest methods to form grids by blocking half the light (creating shadows) and passing the other half of the light. In Fig. 5, a dense grid is written in a biacetyl-laden nitrogen flow by splitting the large ~20 mm diameter high-pulse energy XeFl laser beam into two beams and sending each beam through slits in an aluminum plate [24]. The sheets of laser light emanating from the slits in each plate are focused by a cylindrical lens and crossed in a plane to create the tagging grid (Fig. 27) [24, 91]. By using different width slots in the aluminum plates, they were able to create tag lines with different widths (see Fig. 5) that were easier to track with their spatial correlation (or cross-correlation) software [92]. Other researchers focus the laser into two sheets that pass through aluminum meshes just before crossing in the flow to create a dense grid [44]. Plate or mesh grid formation methods only work well with high-pulse energy lasers and highly phosphorescence tag molecules such as biacetyl in nitrogen [24]. Micro-lens optics are more compact and efficient [2, 16, 38]. In Fig. 25, 7 cylindrical lenses (300 mm f.l., 3 mm x 20 mm) are vertically stacked into each aluminum mount to form HTV girds [69] and none of the laser beam is blocked. A cylindrical lens (300 mm f.l., 20 mm sq.) is horizontally mounted in the front of the stack. The crossed cylindrical lens configuration forms 7 laser beams from each of two optics as sketched in the 7x7 HTV system in Fig. 11 to form 7x7 grid images in Fig. 12. Example 11x11 grids using stacks of 11 micro-lenses (300 mm f.l., 2 mm x 20 mm) are shown in Figs. 1-2.

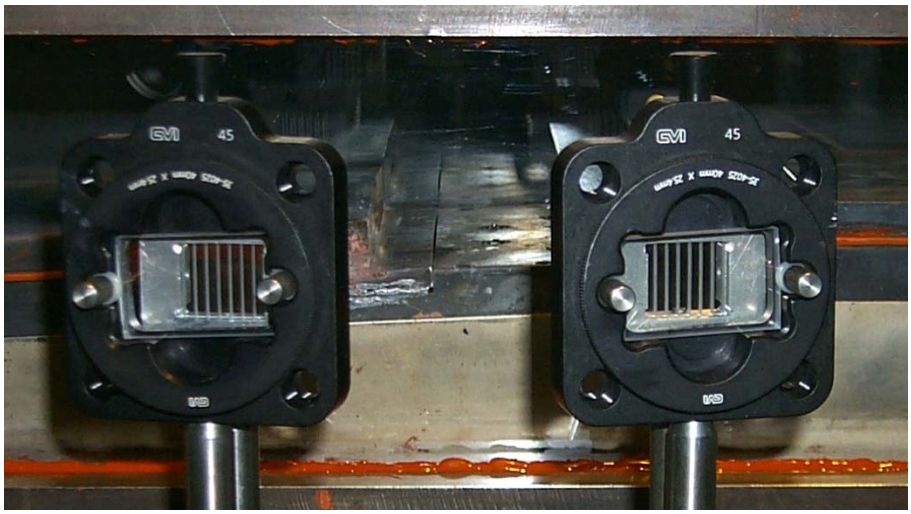

Fig. 25. Grid optics to form a 7x7 grid.

5.2 Planar imaging for 2D velocity

MTV measurements with the multi-line grid forming optics can yield 2D velocity measurements. One example is the 2D velocity field in underexpanded jet using the VENOM and NO fluorescence MTV techniques [44] where the results from VENOM are compared to CFD simulations in Fig. 41 (left) [93]. In another example, the 11x11 HTV system was applied to measure the Mach 2 air

flow behind a strut as shown in Fig. 26 with the strut/cavity geometry (left) and the location of the 11x11 HTV grid (right).

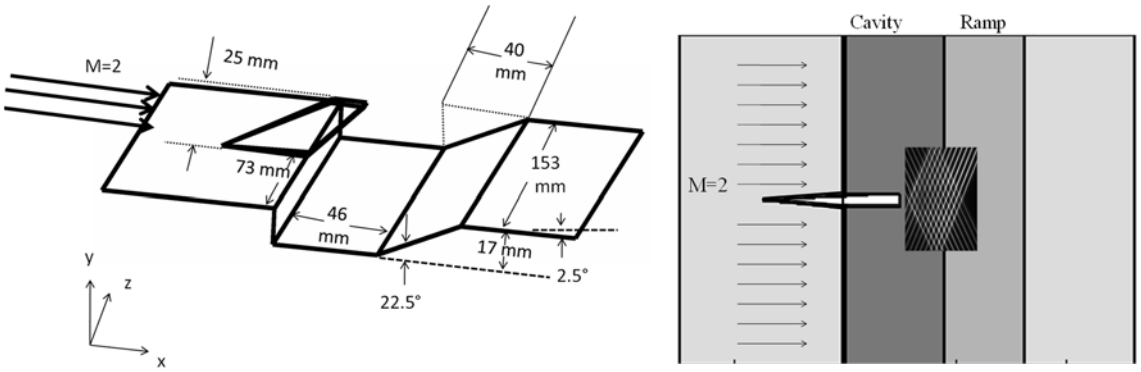

Fig. 26. 2D velocity measurement of a Mach 2 air flow behind a strut/cavity. Left: Flow configuration. Right: 11x11 HTV grid written behind the strut using the HTV system in Fig. 1 [70].

Using an 11 x 11 grid HTV system (Fig. 1), the average 2D velocity measurements and 2D vorticity were compared to large eddy simulations (LES) as shown in Fig. 27 [70]. The measurements and LES model show the same wake flow features including the positive and negative fluid rotation behind the strut [70].

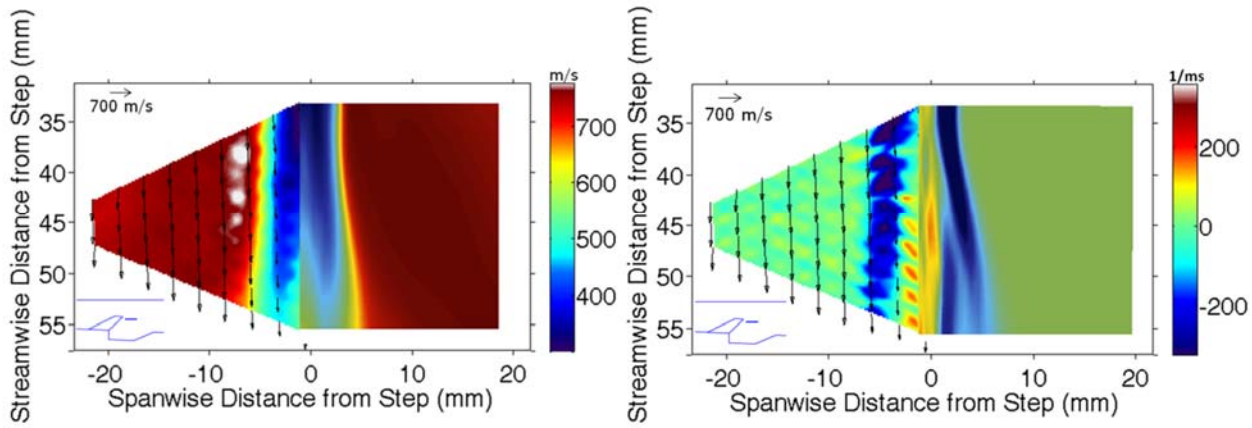

Fig. 27. Measurements of 2D velocity (left) and 2D vorticity (right) where MTV (-z distance) determined by template matching [94] is compared to LES (+z distance) in a Mach 2 air flow behind an upstream strut and cavity at y= 20.3 mm (y=0 is top of cavity, z=0 is strut centerline) [70].

5.3 Stereoscopic 3D Velocity Imaging

A number of researchers have developed 3D velocity MTV systems for gas flows [38, 40, 91, 95]. An example stereoscopic MTV system for measurement of 3D velocity in an automotive cylinder is shown in Figs. 28 and 29 [91]. Mittal et al. premixed a biacetyl/acetone solution into nitrogen gas to study gas flow in an automotive cylinder [91]. As shown in Fig. 28, the XeFl excimer (308 nm, 250 mJ/pulse) is split into two beams and each beam passes through aluminum mesh blockers

to form the tagging grid by biacetyl phosphorescence inside an optically accessible engine cylinder. Measurements of ensemble-averaged 3D velocity at 90 crank angle degrees (CAD) are shown in Fig. 29 (left) and ensemble-averaged out-of-plane vorticity in Fig. 29 (right). At 90 CAD, the piston is about halfway down the cylinder during the intake stroke. The magnitudes of the velocity vectors in Fig. 29 (left) range from 6.7 to 53 m/s. Vedula and co-workers have reviewed the application of MTV to internal combustion (IC) engine flows; they discuss different camera approaches for stereoscopic MTV and their relationship to the accuracy of out-of-plane velocity measurements [96].

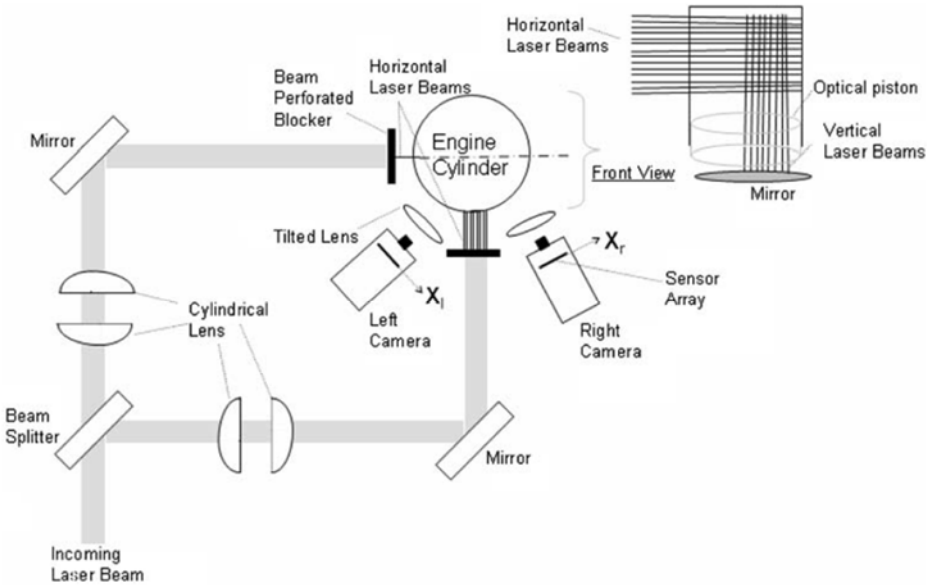

Fig. 28. Stereoscopic MTV system for measurement of in-cylinder flow in an IC engine [91]

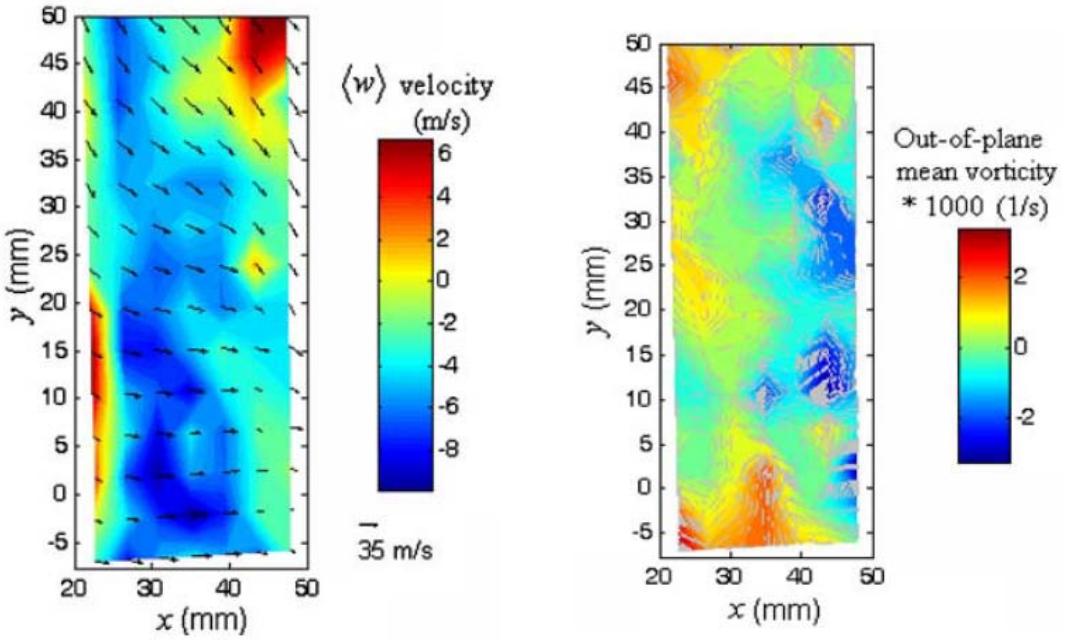

Fig. 29. 3D ensemble-averaged velocity measurements (left) and out-of-plane mean vorticity (right) taken at 90 crank angle degrees by Mittal et al. [91].

6. Analysis Methods for Velocity Determination

6.1 Spatial Correlation Method

Gendrich and Koochesfahani [92] developed a spatial correlation (or cross-correlation) method to determine velocity by finding the displacement of an MTV cross (see Fig. 30 left). The "cross" of the undisplaced tag described by the measured source window intensity I_1 (x, y, t=0) is cross-correlated to the displaced tag described by the measured roam window intensity I_2 (x+Δx, y+Δy, Δt). The values of Δx and Δy are varied until the maximum cross-correlation between I_1 and I_2 is obtained to give the velocity components u=Δx/Δt and v=Δy/Δt [92]. Gendrich and Koochesfahani simulated the tag lines on the camera with Gaussian intensity distributions. Noise was added uniformly over the peak-to-peak values of ±n. The signal-to-noise ratio (SNR) is defined as SNR = S/(2n) where the signal is the contrast (brightest pixel minus darkest pixel). With an MTV image of at least SNR = 4, the grid displacement is determined to less than 0.1 pixels for crossing angles <130° (Fig. 30 right). In this spatial correlation method, distortion of the displaced tag grid by fluid rotation and strain rate is reduced by using a short time delay [92].

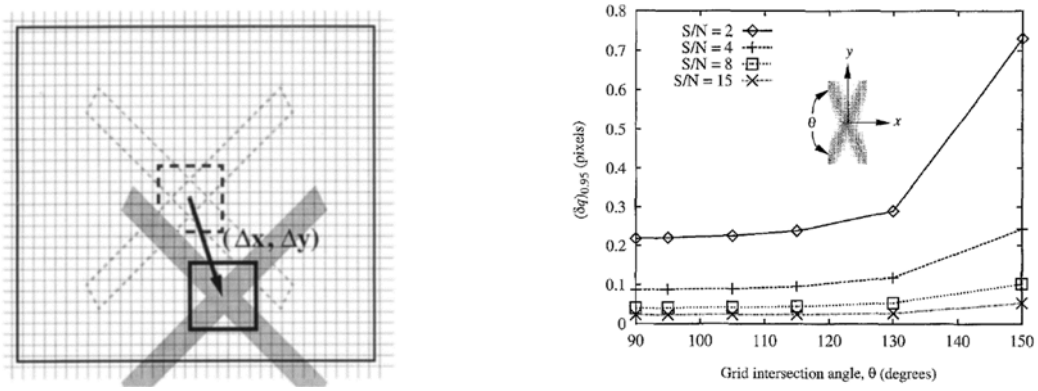

Fig. 30. Spatial correlation (or cross-correlation) method for determining velocity [92]. Left: Undisplaced and displaced tags with source and roam windows. Right: Results of noise simulations showing the measurement accuracy as a function of SNR and grid intersection angle.

7.2 Template Matching Method

Ramsey and Pitz [94] developed a template matching method (see Fig. 31) where a two-segment cross template (defined Gaussian profile segments with length L, width σ_L, intensity I) is fit to the measured tag cross intensity field with an intensity ratio $r=I_2/I_1$ where segment intensity is represented by a Gaussian. This is done for both the undisplaced and displaced tags to determine the template position (x_c, y_c) and segment angles (θ_1, θ_2) of the undisplaced template G and the displaced template G' (Fig. 30 right). Once the templates are fit to the intensity fields by maximizing the cross-correlation, only the templates are used in calculating the tag displacement and tag rotation. Measurements using the template matching method are shown in Fig. 27 for a Mach 2 air flow over an upstream strut over a cavity where one can see the 2D velocity field and 2D vorticity with positive and negative rotation behind the strut [70].

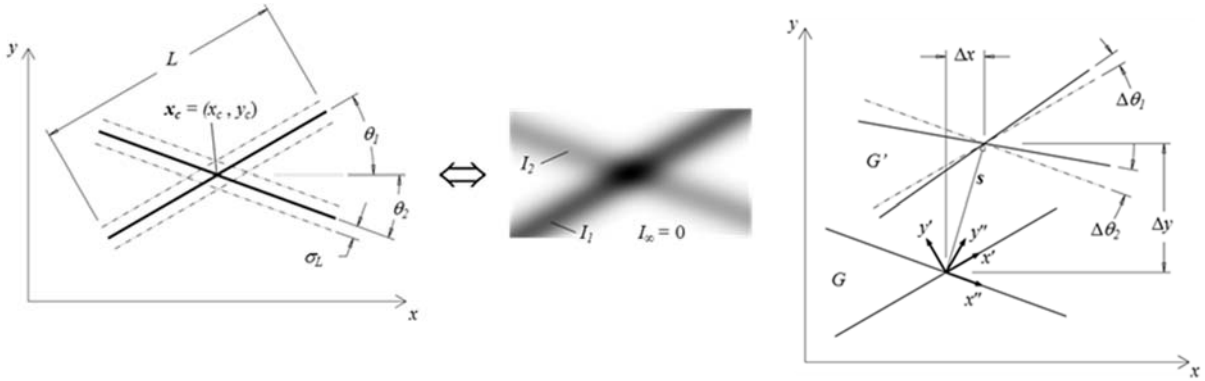

Fig. 31. Template matching method by Ramsey and Pitz [94]. Left: cross template (segment length L, width σ_L) is cross-correlated to MTV grid cross intensity field. Middle: Gaussian distributions of the templates. Right: Template grids G and G' determine fluid displacement and rotation.

Ramsey and Pitz simulated the performance of the template matching method. Uniformly distributed noise was added to the template segment as sketched in Fig. 32. The signal-to-noise ratio SNR defined in Fig. 32 is equivalent to the SNR value used by Gendrich and Koochesfahani.

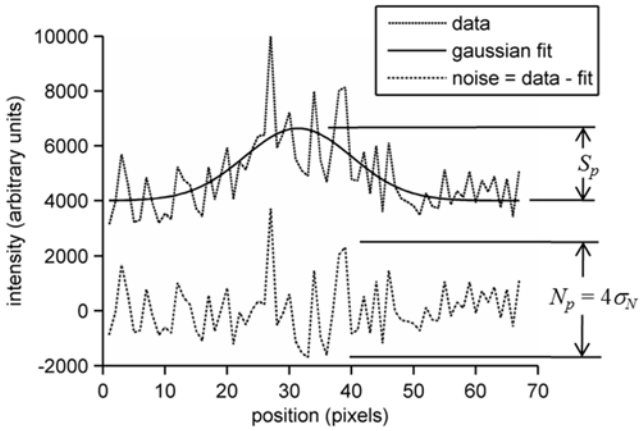

Fig. 32 Simulation of template matching method performance [94]. Bottom curve: the uniformly distributed noise ($\pm$ $2\sigma_N$ range is 95% of the noise and the peak-to-peak value, $N_p = 4\sigma_N$); Top curve: uniform noise distributed over the Gaussian intensity distribution of a segment of the template showing the average signal, S_p. The signal-to-noise ratio is: SNR = $S_p/(4\sigma_N)$. Each point on the noise curve is a pixel value. These segments are shown to be ~15 pixels wide for illustration purposes.

For lower intensity, less-resolved MTV grids measured in gases (as opposed to bright MTV grids using photochromic dyes in liquids [97]), the template matching method is more accurate giving a lower displacement error compared to cross-correlation as seen in Fig. 33 (left) [94]. Also allowing template segments to rotate during displacement gives accurate displacement measurement in rotational flow unlike the cross-correlation method [92] whose accuracy decreases with flow rotation. If the flow is strongly rotational, the displacement error from the cross-correlation method noticeably increases (Fig. 33 left, cross-correlation curves for rotational and irrotational flow [94]) while the template method shows no effect from the fluid rotation. With template matching and an MTV grid SNR = 4 or greater, the linear displacement is measured to less than 0.1 pixel and the angular displacement to less than 0.02 radians (Fig. 33 right).

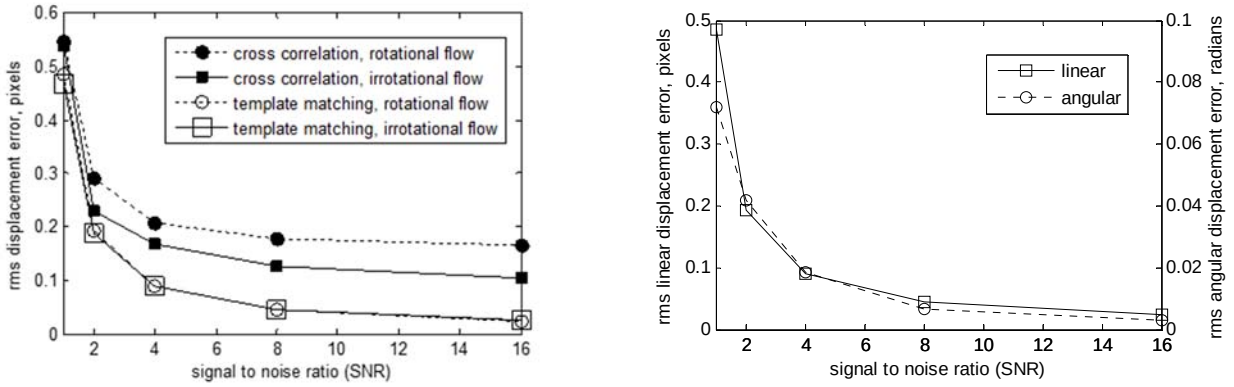

Fig. 33. Template matching method [94]. Left: Displacement rms error for cross-correlation (spatial correlation) and template matching methods in irrotational and rotational flow. The template matching method maintains its accuracy under fluid rotation. Right: Linear and angular displacement errors for template matching.

6.3 Image Correlation Velocimetry (ICV)

Higher order grid tracking schemes such as Image Correlation Velocimetry (ICV) [75] can derive a high fidelity velocity field from the convection of the grid. For example in Fig. 14, the 120 velocity vector field is determined by ICV from a 3x3 OTV grid [16] whereas the spatial correlation and template matching methods described above would yield only 9 velocity vectors at the grid crossing points.

The ICV method developed by Tokumaru and Dimotakis [75] uses B-splines to describe the transformation of the undisplaced grid to the displaced grid by convection. For MTV grids, the primary information is in the crossing points of the grid and the number of parameters needed to specify the B-splines must not exceed the number of (x,y) crossing points described by the grid. This is illustrated in Fig. 34 for a 3x3 grid that has 3x3x2 = 18 coordinate values [16]. The best fit is the center image with an 18-parameter fit whereas the right-hand image using a 32-parameter fit gives nonsensical results.

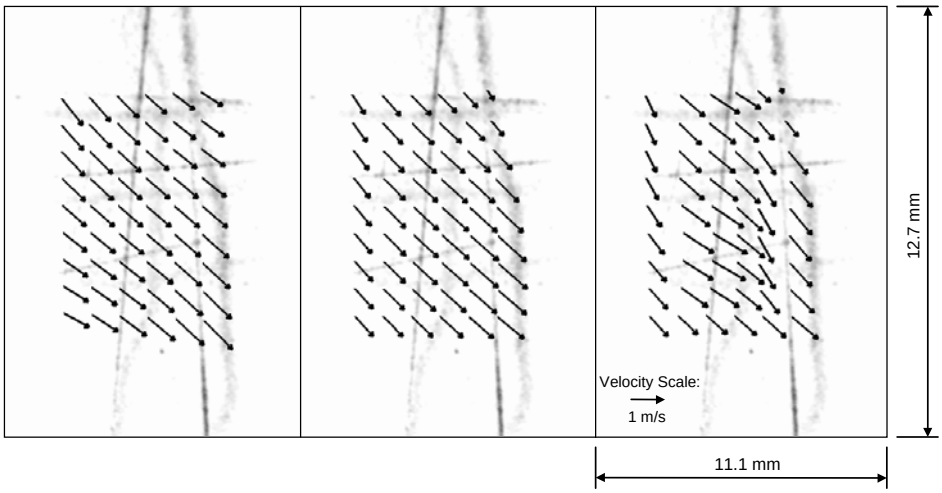

Fig. 34. Image Correlation Velocimetry (ICV) B-spline fits of 3x3 ozone tagging velocimetry (OTV) grids containing 3x3x2=18 information coordinates [16]. Left: single patch using bilinear B-splines with 8-parameter fit. Center: single patch using bi-quadratic B-spines with 18-parameter fit. Right: 2x2 bi-quadratic B-spline patches with 32-parameter fit.

7. Uncertainty of MTV

When measuring the 2-D velocity using an MTV grid, the velocity components in the gas are given by [37]:

$$u = M\,\frac{\Delta x}{\Delta t} \qquad ; \qquad v = M\,\frac{\Delta y}{\Delta t} \tag{11}$$

where M is the camera magnification (mm/pixel) and (Δx, Δy) are tag displacements (pixels) as shown in Fig. 30 (left). The magnification should be chosen such that the tag is ~5 pixels wide in order to determine its position to <0.1 pixel accuracy (for SNR≥4) while keeping a sufficient field-of-view. The tag delays should be long enough to allow ~10 pixel displacements. For typical MTV systems, the laser lines will be written ~0.5 mm wide with diffusion increasing the tag width with time. Thus, a magnification of 0.1 mm/pixel will give 5 pixel wide tag lines and a 10 cm x 10 cm field of view for a 1000 x 1000 pixel camera. A 10 pixel displacement needed for accurate displacement measurement will be 1 mm. A calibrated spatial target placed in the image plane of the camera should allow M to be determined at each pixel location (x,y) to better than 1% accuracy.

The velocity components (u,v) measured with MTV are averaged over the tag displacement. Thus the spatial resolution of the MTV measurement is (Δx, Δy).

For an MTV system based on Eqn. 11, the uncertainty of u and v components of the MTV system are [98],

$$\frac{\sigma_u}{u} = \sqrt{\left(\frac{\sigma_M}{M}\right) + \left(\frac{\sigma_{\Delta x}}{\Delta x}\right) + \left(\frac{\sigma_{\Delta t}}{\Delta t}\right)} \quad ; \quad \frac{\sigma_v}{v} = \sqrt{\left(\frac{\sigma_M}{M}\right) + \left(\frac{\sigma_{\Delta y}}{\Delta y}\right) + \left(\frac{\sigma_{\Delta t}}{\Delta t}\right)} \tag{12}$$

where σ_M, $\sigma_{\Delta x}$, $\sigma_{\Delta y}$, and $\sigma_{\Delta t}$ are 95% confidence uncertainties in M, Δx, Δy, and Δt.

For most MTV systems, the relative uncertainty in measuring the tag displacement is the greatest. The magnification uncertainty is less than 1% [37] and if the tag is imaged with a 2nd laser using a short-gate intensified CCD camera, the timing error is small [69] and the velocity errors are:

$$\frac{\sigma_u}{u} = \frac{\sigma_{\Delta x}}{\Delta x} \quad ; \quad \frac{\sigma_v}{v} = \frac{\sigma_{\Delta y}}{\Delta \mathrm{y}} \tag{13}$$

As seen in Fig. 33 for template matching, for SNR > 4, the displacement error is <0.1 pixel. Thus, for a 10 pixel displacement, the velocity measurement accuracy can approach ±1%.

For example, HTV 7x7 grid measurements (SNR ≥ 7) applied to a Mach 2 supersonic air flow in Research Cell 19 at the US Air Force Research Laboratory have single-shot uncertainties of ±1% (±8 m/s) and measure freestream turbulence levels of 2% (±15 m/s) for a freestream velocity of 700 m/s. In the freestream measurements the time delays are 2-3 μs with corresponding spatial resolutions (tag displacements) in the streamwise direction of 1.4-2.1 mm [69].

When using a single MTV line (e.g., Figs. 7, 8, 17) to measure the streamwise velocity instead of a grid, an additional uncertainty is introduced due to the effect of the spanwise velocity,

$$\frac{\sigma_u}{u} \cong \Delta t \frac{v'_{rms}}{U} \frac{dU}{\mathrm{dy}} \tag{14}$$

where U is the freestream velocity, v'_{rms} is the rms level of the cross-stream velocity, and $\frac{dU}{dy}$ is the average gradient in the streamwise velocity [32, 99, 100]. For example, when applying single-line Krypton tagging velocimetry (KTV) to measure a 1400 m/s freestream velocity in AEDC Wind Tunnel 9, Mustafa and co-workers determined the measurement had a single-shot uncertainty of ±3% where most of the uncertainty is due the spanwise uncertainty term (Eqn. 14) for 5% freestream turbulence [100].

In single-laser methods based on LIF (see Fig. 7), the fluorescence signal decays by collisional quenching requiring a longer camera exposure time to record the tag locations leading to more temporal uncertainty and a perceived shift in the delayed tag image that must be corrected [32]. To estimate a measurement technique's accuracy, one should compare the method against an accepted standard measurement technique. Unfortunately, such reference techniques are rarely available. Instead the MTV accuracy can be estimated in "no-flow" or quiescent tests [32, 35] although such tests do not fully assess these uncertainties. Using single-line, single-laser NO fluorescence tagging, Bathel and co-workers determined that the velocity accuracy is ±10 m/s and precision is ~25 m/s for pressures near 500 Pa in a wind tunnel with "no-flow" conditions as seen in Fig. 35 [32]. When single-line, single-laser NO fluorescence MTV is applied to the 31 inch Langley Mach 10 air tunnel (~1000 m/s), uncertainties of ±2.7% (±30 m/s) are obtained for 40 image-averages and the single-shot uncertainties are estimated to be ±9.7% (±100 m/s) based on 95% confidence [32].

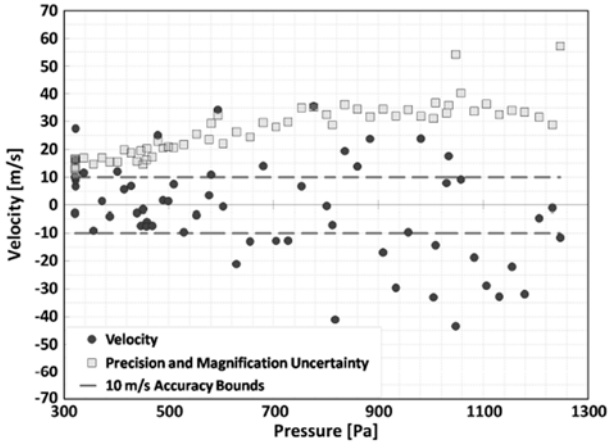

Fig. 35. Velocity accuracy data obtained from low pressure "no-flow" wind tunnel test using single-line, single-laser NO-MTV [32].

Low-speeds need to be measured in gas-cooled nuclear reactors and Andre et al. applied N_2O MTV to measure gas velocities below 1 m/s with delay times of up to 40 ms [37]. For these long time delays, tag heating could lead to buoyancy effects that bias the measurements. Andre and coworkers [37] determined that in their NO_2-NO MTV experiment the temperature increase would be less than 3 K resulting in a 0.004 m/s change in the velocity during their 40 ms measurement time. Since these buoyancy effects are difficult to quantify, the N_2O MTV measurements are quantified in terms of their precision. The precision of N_2O photodissociation MTV can be as low as 0.004 m/s at time delays of 40 ms as shown in Fig. 36. At 40 ms delay, the buoyancy error and the measurement precision are comparable.

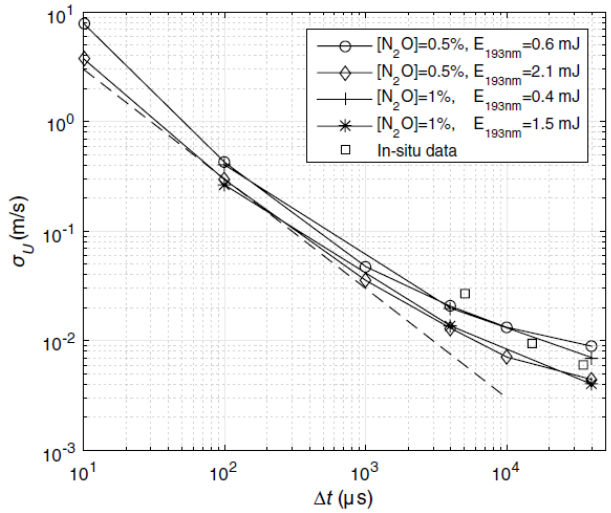

Fig. 36. Precision of N_2O MTV measurement in a gas jet for time delays up to 40 ms where the precision is as low as 0.004 m/s. In-situ data are shown from an integral effect test facility for the study of gas-cooled nuclear reactors [37].

8. Applications

8.1 Supersonic Flow over a Cavity

HTV has been applied to measure supersonic flow over a rectangular-walled cavity [69], wall-ramp cavity and an upstream strut over a wall-ramp cavity using the HTV system (Fig. 1). Measured velocities are compared to large-eddy simulations (LES) in Fig. 37. 2D mean velocity and 2D vorticity behind the strut are shown in Fig. 27.

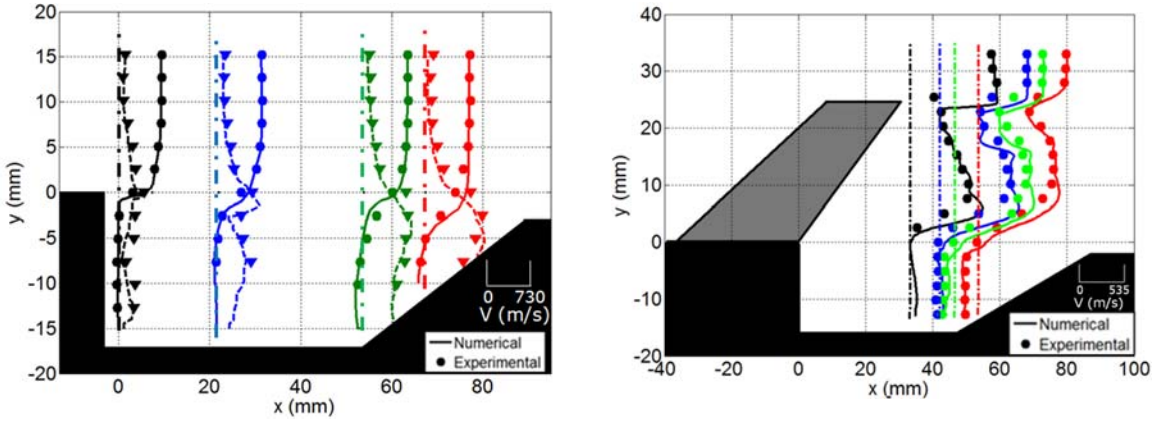

Fig. 37. HTV measurements of Mach 2 supersonic flow over a wall/cavity (left) and behind an upstream strut over a wall/cavity compared to large-eddy simulations (LES). Left: Mean (dots) and RMS (triangles) velocities are compared to LES (lines, dotted lines). Right: Mean velocity (dots) are compared to LES (lines). Vertical dashed-dotted lines indicate the streamwise measurement locations [70].

8.2 Laminar and Turbulent Flames

HTV produces an OH tag that has been used to measure velocities in laminar flames (Fig. 12) [66] and in turbulent flames (Fig. 38) [1]. A 3x3 HTV grid written 40 mm downstream of a N_2-diluted H_2 turbulent jet diffusion flame issuing into room air is shown in Fig. 38 (left). The velocity vector in the center is 22 m/s where the OH background from the flame is significant but the HTV grid is still seen. An 11x11 HTV grid written into the plume of a propane-air torch is visible in Fig. 38 (middle) with background OH. The OH background can be reduced at high temperatures by using VE-HTV as shown in Fig. 18.

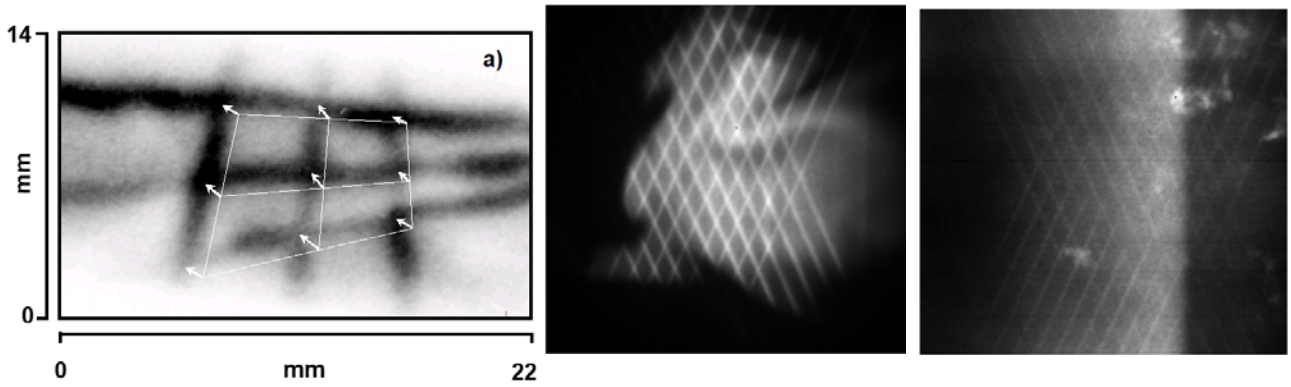

Figure 38. HTV grid images in flames. Left: 3x3 HTV grid written into an N_2-diluted H_2 turbulent jet diffusion flame issuing into room air (1.8 mm dia., 10 SLPM of N_2, 40 SLPM of H_2). The image is taken ~40 mm downstream and the central vector is 22 m/s [1]. Middle: 11x11 HTV grid written into the plume from a propane-air torch with background OH. Right: HTV grid written into an airflow over ethylene-air step-cavity flame [middle and right are previously unpublished].

Although HTV grids in methane and propane flames are visible, measurements in other hydrocarbon (HC) flames can be difficult. Some hydrocarbon molecules directly absorb the 193-nm ArF laser light and flame emission can overwhelm the OH LIF. An HTV grid formed in a rich ethylene-air flame formed behind a step/cavity is shown in Fig. 38 right. The HTV grid is barely visible due to the increased background OH and the direct absorption of the 193-nm beam by the ethylene fuel. This can also be seen in recent HTV measurements by Ye et al. who passed a 193-nm ArF beam through the air-region, fuel-region, and reaction-region of a kerosene-fueled dual-mode scramjet combustor [73]. They were only able to measure velocity using HTV when the ArF laser passed through pure air-regions of the scram-jet flowfield [73].

8.3 Rocket Plumes

Velocity measurements are needed in rocket plumes to validate simulations. During rocket engine start-up, a complex plume pattern called a "cap-shock" pattern (Fig 39, left) occurs in thrust-optimized nozzles that is difficult to numerically simulate and can lead to destructive combustion instabilities [74]. The outer annulus of the plume is supersonic and surrounds a normal shock (called a Mach Stem MS) followed by a subsonic flow with a possible recirculating "trapped" vortex [101]. Hydroxyl tagging velocimetry was applied to measure the cap shock pattern of a small liquid hydrogen peroxide monopropellant rocket engine [74]. The HTV tag lines measured in the rocket plume are shown in Fig. 39 (right). The OH tags are brighter in the subsonic region behind the Mach Stem (MS) that has a temperature approaching the stagnation temperature (1041 K). The ~1500 m/s outer supersonic plume produces large tag line displacements while behind the Mach Stem (MS) the flow is subsonic.

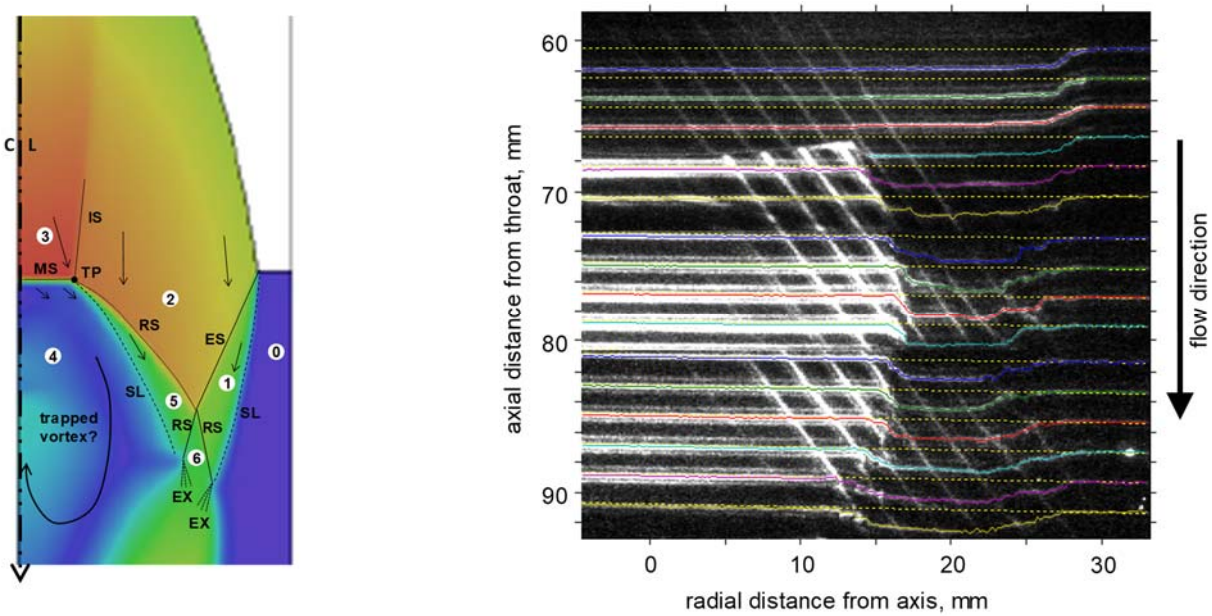

Fig. 39. HTV measurements in the cap shock pattern during engine start-up in a thrust-optimized rocket plume [74]. Left: Schematic showing outer supersonic annular jet, inner normal shock, Mach stem, and possible subsonic trapped recirculating vortex. The waves, regions, and shading follow that from Hagemann and Frey [101] (CL=center-line, EX=expansion fan, IS=internal shock, MS=Mach stem, RS=reflected shock, SL=slip line, TP=triple point). Right: HTV lines written into the plume. (Dashed lines indicate original positions of horizontal HTV lines and three single-shot images are stitched together at different downstream locations.)

The measured mean velocity pattern in the rocket plume is shown in Fig. 40 (left). The crossing HTV tag lines result in the individual velocity vectors and the shading represents the mean streamwise velocity from the horizontal tag lines. The measured velocity pattern is compared to CFD simulations in Fig. 40 (right) and both show the cap shock pattern. Behind the Mach Stem (MS), CFD simulations predict flow recirculation also found in previous numerical simulations by Hagemann and Frey [101]. The HTV measurements show no recirculation and a broader diameter

plume (i.e., more fully flowing nozzle) than the CFD results. The lack of recirculation is consistent with recent measurements in an under-expanded jet Mach disk [102].

In Fig. 40, the Mach Stem (MS) regions are shaded out due to loss of HTV data. First, a linear interpolation across a normal shock is nonsensical. Secondly, one of the HTV lines disappears when it crosses the normal shock.

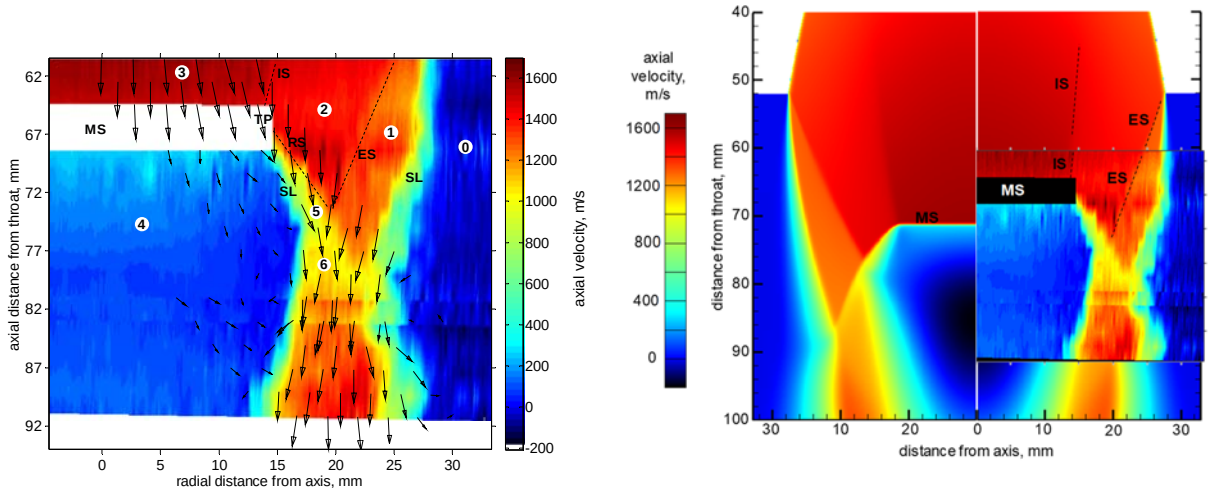

Fig. 40. HTV measurements (left, right inset) vs. CFD predictions of a H_2O_2-liquid rocket plume with stagnation chamber at 19.9 bar, 1041 K. Rocket nozzle with 55.3 mm exit diameter and 7.4 area ratio [74]. Numbered regions (left) correspond to same regions in Fig. 38 left.

9.0 Combining MTV with other Spectroscopic Methods

Besides velocity, molecular tags can be used to measure other gas properties such as temperature, concentration, and mixture fraction [103-105]. The NO fluorescence MTV and VENOM techniques have been combined with two-line NO fluorescence to measure velocity and temperature [77, 93, 95]. The VENOM technique measured simultaneous velocity and temperature in an underexpanded jet flowfield as shown in Fig. 41. After the vibrationally excited $NO_{v=1}$ tag is created by photodissociation of NO_2 by a 355-nm laser, two UV dye lasers are used to make a two-line rotational temperature measurement NO tag by LIF [77, 93].

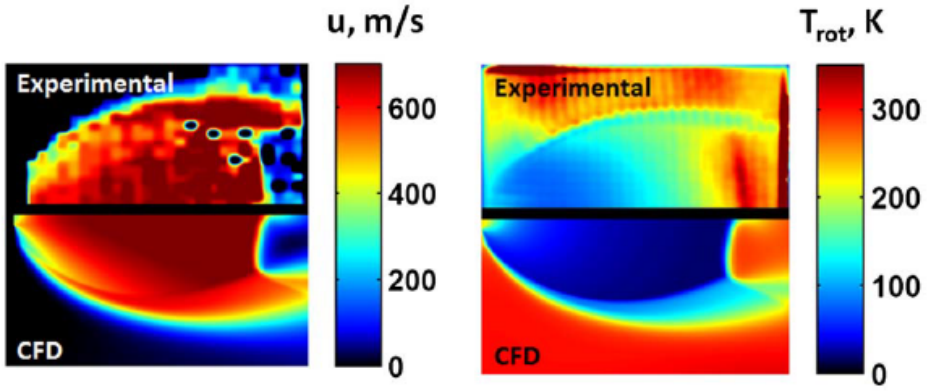

Fig. 41. Simultaneous streamwise velocity and rotational temperature of the flowfield of an under-expanded jet of nitrogen (6.3% NO_2) measured by the VENOM technique and compared to CFD simulations [93].

Since MTV does not use particles, MTV can be combined with other molecular techniques such as LIF, Raman scattering, and Rayleigh scattering. Hu and co-workers combined vibrational Raman spectroscopy with HTV to make simultaneous measurements of temperature, chemical composition (H_2, H_2O, O_2, N_2), and temperature in a Hencken Burner and above a lifted turbulent jet diffusion flame of hydrogen into still air [106]. The HTV grid formed in the Hencken Burner superimposed on the KrF laser beam used for line Raman scattering is shown in Fig. 42. Single-shot measurements of velocity, temperature, and chemical composition at a location 30 cm (150 dia.) above the lifted turbulent jet diffusion flame are shown in Fig. 43. The Raman data is along an 8.4 mm line (0.4 mm spatial resolution). At this location, all of the H_2 fuel in the jet has been converted to H_2O.

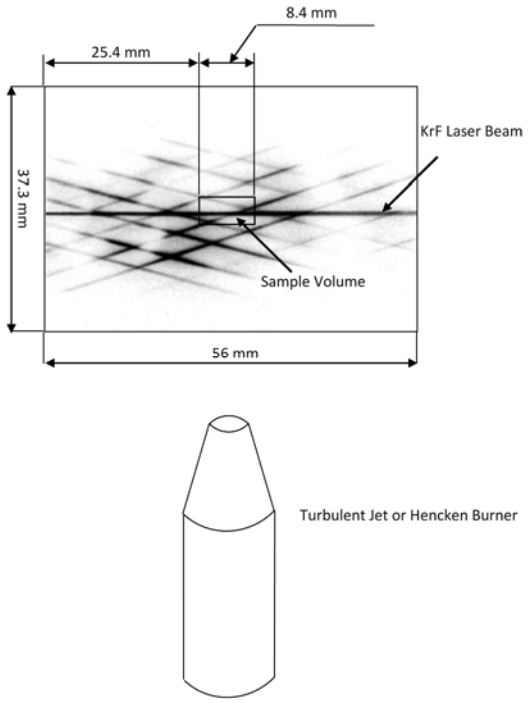

Fig. 42. Combined HTV and Raman scattering system for velocity, species and temperature measurements over a Hencken Burner Flame or Turbulent Jet Flame. The HTV grid created in the Hencken Burner Flame overlaps the strong OH LIF produced by photodissociation of H_2O by the KrF excimer laser beam used for the vibrational Raman scattering. The KrF laser 8.4 mm line segment used for line Raman scattering sampling (0.4 mm spatial resolution) is shown [106].

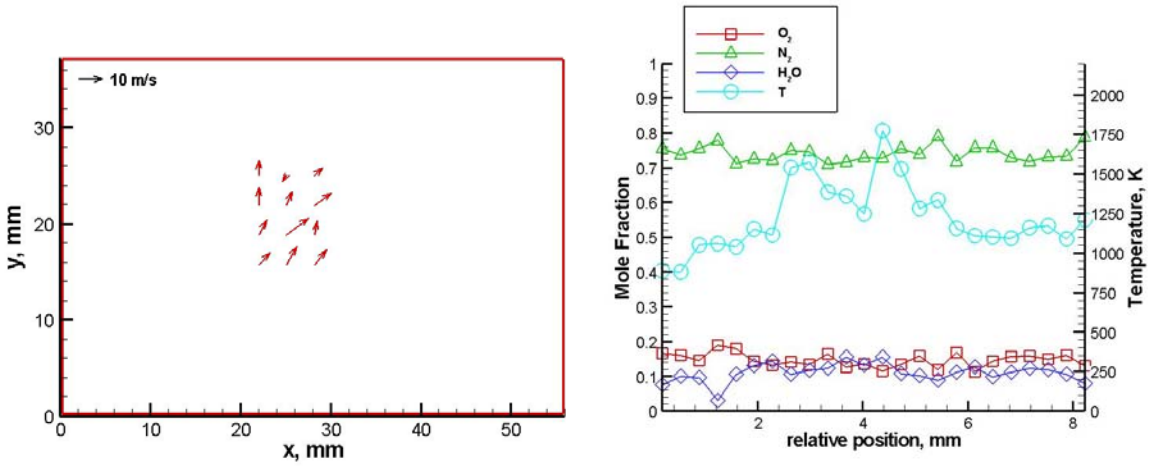

Fig. 43. Simultaneous velocity, temperature, and species concentrations (H_2, H_2O, O_2, N_2) above a lifted H_2 turbulent jet diffusion flame into still air. Data taken at 30 cm (150 dia.) downstream of the jet exit (1.8 mm jet dia., exit velocity 360 m/s). H_2 fuel is absent at this downstream location [106].

9. Conclusions

This chapter has described many different single-laser and multi-laser molecular tagging velocimetry (MTV) methods. References were provided for dozens of different molecules and excitation schemes and several examples were provided for different molecules, some of which need to be seeded into a flow and others of which occur naturally such as O_2, N_2 or water vapor.

Various methods of exciting points, lines, crosses, and grids are discussed along with examples of 2D and 3D velocity flowfield measurements. Measurement uncertainty is specifically addressed with common error sources identified as well as methods for reducing these errors such as improving signal-to-noise ratio, increasing the inter-frame acquisition time, using appropriate magnification that optimizes accuracy/field-of-view, and using advanced image processing techniques. However, tradeoffs are described that must be balanced (e.g. measurement uncertainty is inversely proportional to the inter-frame time while the spatial resolution is proportional to the inter-frame time). Finally, the chapter concludes with examples in high-speed supersonic and propulsion flows as well as examples of combining MTV with other spectroscopic methods.

References

[1] J.A. Wehrmeyer, L.A. Ribarov, D.A. Oguss, R.W. Pitz, Flame flow tagging velocimetry with 193-nm H_2O photodissociation, Applied Optics 38 (1999) 6912-6917.
[2] M.D. Lahr, R.W. Pitz, Z.W. Douglas, C.D. Carter, Hydroxyl-tagging-velocimetry measurements of a supersonic flow over a cavity, Journal of Propulsion and Power 26 (2010) 790-797.
[3] C. Tropea, A.L. Yarin, J.F. Foss, Handbook of Experimental Fluid Mechanics, Springer, Berlin, 2007.
[4] O.J.H. Williams, T. Nguyen, A.M. Schreyer, A.J. Smits, Particle response analysis for particle image velocimetry in supersonic flows, Physics of Fluids 27 (2015).
[5] T. Sakurai, T. Handa, S. Koike, K. Mii, A. Nakano, Study on the particle traceability in transonic and supersonic flows using molecular tagging velocimetry, Journal of Visualization 18 (2015) 511-520.
[6] R.E. Huffman, Jr., G.S. Elliott, An experimental investigation of accurate particle tracking in supersonic, rarefied axisymmetric jets, 47th AIAA Aerospace Sciences Meeting, Paper No. AIAA-2009-1265, Orlando, Florida, USA, 2009.
[7] R.J. Santoro, S. Pal, R.D. Woodward, L. Schaaf, Rocket testing at university facilities, 39th AIAA Aerospace Sciences Meeting, Paper No. AIAA-2001-0748, Reno, Nevada, USA, 2001.
[8] M.M. Koochesfahani, D.G. Nocera, Molecular Tagging Velocimetry (MTV), in: C. Tropea, A.L. Yarin, J.F. Foss (Eds.), Handbook of Experimental Fluid Mechanics, Springer, Berlin, 2007.
[9] N. Dam, R.J.H. Klein-Douwel, N.M. Sijtsema, J.J. ter Meulen, Nitric oxide flow tagging in unseeded air, Optics Letters 26 (2001) 36-38.
[10] J.B. Michael, M.R. Edwards, A. Dogariu, R.B. Miles, Femtosecond laser electronic excitation tagging for quantitative velocity imaging in air, Applied Optics 50 (2011) 5158-5162.
[11] M.R. Edwards, A. Dogariu, R.B. Miles, Simultaneous Temperature and Velocity Measurements in Air with Femtosecond Laser Tagging, AIAA Journal 53 (2015) 2280-2288.
[12] L.R. Boedeker, Velocity-measurement by H_2O photolysis and laser-induced fluorescence of OH, Optics Letters 14 (1989) 473-475.
[13] L.P. Goss, T.H. Chen, D.D. Trump, B. Sarka, Flow-tagging velocimetry using UV-photodissociation of water vapor, 29th AIAA Aerospace Sciences Meeting, Paper No. AIAA-1991-0335, Reno, Nevada, USA, 1991.
[14] N. Grady, R.W. Pitz, Vibrationally excited hydroxyl tagging velocimetry, Applied Optics 53 (2014) 7182-7188.
[15] R.W. Pitz, T.M. Brown, S.P. Nandula, P.A. Skaggs, P.A. DeBarber, M.S. Brown, J. Segall, Unseeded velocity measurement by ozone tagging velocimetry, Optics Letters 21 (1996) 755-757.
[16] R.W. Pitz, J.A. Wehrmeyer, L.A. Ribarov, D.A. Oguss, F. Batliwala, P.A. DeBarber, S. Deusch, P.E. Dimotakis, Unseeded molecular flow tagging in cold and hot flows using ozone and hydroxyl tagging velocimetry, Measurement Science & Technology 11 (2000) 1259-1271.
[17] L.A. Ribarov, J.A. Wehrmeyer, F. Batliwala, R.W. Pitz, P.A. DeBarber, Ozone tagging velocimetry using narrowband excimer lasers, AIAA Journal 37 (1999) 708-714.
[18] R.B. Miles, J.J. Connors, E.C. Markovitz, P.J. Howard, G.J. Roth, Instantaneous profiles and turbulence statistics of supersonic free shear layers by Raman excitation plus laser-induced electronic fluorescence (RELIEF) velocity tagging of oxygen, Experiments in Fluids 8 (1989) 17-24.
[19] R.B. Miles, D.Y. Zhou, B.Y. Zhang, W.R. Lempert, Z.S. She, Fundamental turbulence measurements by RELIEF flow tagging, AIAA Journal 31 (1993) 447-452.

[20] A. Noullez, G. Wallace, W. Lempert, R.B. Miles, U. Frisch, Transverse velocity increments in turbulent flow using the RELIEF technique, Journal of Fluid Mechanics 339 (1997) 287-307.
[21] C.A. Hall, M.C. Ramsey, D.A. Knaus, R.W. Pitz, Molecular tagging velocimetry in nitrogen with trace water vapor, Measurement Science and Technology 28 (2017) 085201.
[22] S.H. Zhang, X.L. Yu, H. Yan, H.J. Huang, H.L. Liu, Molecular tagging velocimetry of NH fluorescence in a high-enthalpy rarefied gas flow, Applied Physics B-Lasers and Optics 123 (2017).
[23] W.R. Lempert, N. Jiang, S. Sethuram, M. Samimy, Molecular tagging velocimetry measurements in supersonic microjets, AIAA Journal 40 (2002) 1065-1070.
[24] B. Stier, M.M. Koochesfahani, Molecular tagging velocimetry (MTV) measurements in gas phase flows, Experiments in Fluids 26 (1999) 297-304.
[25] B. Hiller, R.A. Booman, C. Hassa, R.K. Hanson, Velocity visualization in gas-flows using laser-induced phosphorescence of biacetyl, Review of Scientific Instruments 55 (1984) 1964-1967.
[26] R.J. Balla, Iodine Cordes Bands Thermometry in a Mach 10 Wake, AIAA Journal 52 (2014) 2901-2903.
[27] N.J. Parziale, M.S. Smith, E.C. Marineau, Krypton tagging velocimetry of an underexpanded jet, Applied Optics 54 (2015) 5094-5101.
[28] M.A. Mustafa, D. Shekhtman, N.J. Parziale, Single-laser krypton tagging velocimetry investigation of supersonic air and N_2 boundary-layer flows over a hollow cylinder in a shock tube, Physical Review Applied 11 (2019) 064013.
[29] P. Barker, A. Thomas, H. Rubinsztein-Dunlop, P. Ljungberg, Velocity measurements by flow tagging employing laser enhanced ionisation and laser induced fluorescence, Spectrochimica Acta Part B-Atomic Spectroscopy 50 (1995) 1301-1310.
[30] A.F.P. Houwing, D.R. Smith, J.S. Fox, P.M. Danehy, N.R. Mudford, Laminar boundary layer separation at a fin-body junction in a hypersonic flow, Shock Waves 11 (2001) 31-42.
[31] P.M. Danehy, S. O'Byrne, A.F.P. Houwing, J.S. Fox, D.R. Smith, Flow-tagging velocimetry for hypersonic flows using fluorescence of nitric oxide, AIAA Journal 41 (2003) 263-271.
[32] B.F. Bathel, P.M. Danehy, J.A. Inman, S.B. Jones, C.B. Ivey, C.P. Goyne, Velocity profile measurements in hypersonic flows using sequentially imaged fluorescence-based molecular tagging, AIAA Journal 49 (2011) 1883-1896.
[33] C. Orlemann, C. Schulz, J. Wolfrum, NO-flow tagging by photodissociation of NO_2. A new approach for measuring small-scale flow structures, Chemical Physics Letters 307 (1999) 15-20.
[34] A.G. Hsu, R. Srinivasan, R.D.W. Bowersox, S.W. North, Molecular tagging using vibrationally excited nitric oxide in an underexpanded jet flowfield, AIAA Journal 47 (2009) 2597-2604.
[35] B.F. Bathel, P.M. Danehy, S.B. Jones, C.T. Johansen, C.P. Goyne, Trip-induced transition measurements in a hypersonic boundary layer using molecular tagging velocimetry, 51st AIAA Aerospace Sciences Meeting, Paper No. AIAA-2013-0042, Dallas, Texas, USA, 2013.
[36] A.M. ElBaz, R.W. Pitz, N_2O molecular tagging velocimetry, Applied Physics B-Lasers and Optics 106 (2012) 961-969.
[37] M.A. Andre, R.A. Burns, P.M. Danehy, S.R. Cadell, B.G. Woods, P.M. Bardet, Development of N_2O-MTV for low-speed flow and in-situ deployment to an integral effect test facility, Experiments in Fluids 59 (2018).
[38] S. Kruger, G. Grunefeld, Stereoscopic flow-tagging velocimetry, Applied Physics B-Lasers and Optics 69 (1999) 509-512.
[39] B.F. Bathel, P.S. Iyer, K. Mahesh, P.M. Danehy, J.A. Inman, S.B. Jones, C.T. Johansen, Comparing experiment and computation of hypersonic laminar boundary layers with isolated roughness, 52nd Aerospace Sciences Meeting, Paper AIAA-2014-0236, National Harbor, Maryland, USA, 2014.
[40] P.M. Danehy, B.F. Bathel, N. Calvert, A. Dogariu, R.P. Miles, Three-component velocity and acceleration measurement using FLEET, 30th AIAA Aerodynamic Measurement Technology and Ground Testing Conference, Paper No. AIAA-2014-2228, Atlanta, Georgia, USA, 2014.
[41] R.A. Burns, P.M. Danehy, Unseeded velocity measurements around a transonic airfoil using femtosecond laser tagging, AIAA Journal 55 (2017) 4142-4154.
[42] R.A. Burns, P.M. Danehy, B.R. Halls, N.B. Jiang, Femtosecond laser electronic excitation tagging velocimetry in a transonic, cryogenic wind tunnel, AIAA Journal 55 (2017) 680-685.
[43] R.A. Burns, C.J. Peters, P.M. Danehy, Unseeded velocimetry in nitrogen for high-pressure, cryogenic wind tunnels, part I: femtosecond-laser tagging, Measurement Science and Technology 29 (2018) 115302.
[44] A.G. Hsu, R. Srinivasan, R.D.W. Bowersox, S.W. North, Two-component molecular tagging velocimetry utilizing NO fluorescence lifetime and NO_2 photodissociation techniques in an underexpanded jet flowfield, Applied Optics 48 (2009) 4414-4423.

[45] K.F. Cabell, K.E. Rock, A finite rate chemical analysis of nitric oxide flow contamination effects on scramjet performance, NASA/TP-2003-21259, 2003.
[46] R.A. Parker, T. Wakeman, M. MacLean, M. Holden, Measuring nitric oxide freestream velocity using a quantum cascade laser at CUBRC, 45th Aerospace Sciences Meeting, Paper No. AIAA-2003-1329, Reno, Nevada, USA, 2007.
[47] J.A. Inman, B.F. Bathel, C.T. Johansen, P.M. Danehy, S.B. Jones, J.G. Gragg, S.C. Splinter, Nitric-oxide planar laser-induced fluorescence measurements in the hypersonic materials environmental test system, AIAA Journal 51 (2013) 2365-2379.
[48] E.R. Lachney, N.T. Clemens, PLIF imaging of mean temperature and pressure in a supersonic bluff wake, Experiments in Fluids 24 (1998) 354-363.
[49] B.F. Bathel, P.M. Danehy, C.T. Johansen, S.B. Jones, C.P. Goyne, Hypersonic boundary layer measurements with variable blowing rates using molecular tagging velocimetry, 28th AIAA Aerodynamic Measurement Technology, Ground Testing, and Flight Testing Conference, Paper No. AIAA-2012-2886, New Orleans, Louisiana, USA, 2012.
[50] R. Sanchez-Gonzalez, R.D.W. Bowersox, S.W. North, Vibrationally excited NO tagging by NO (A^2 $Sigma^+$) fluorescence and quenching for simultaneous velocimetry and thermometry in gaseous flows, Optics Letters 39 (2014) 2771-2774.
[51] N.B. Jiang, B.R. Halls, H.U. Stauffer, P.M. Danehy, J.R. Gord, S. Roy, Selective two-photon absorptive resonance femtosecond-laser electronic-excitation tagging velocimetry, Optics Letters 41 (2016) 2225-2228.
[52] N.B. Jiang, J.G. Mance, M.N. Slipchenko, J.J. Felver, H.U. Stauffer, T.X. Yi, P.M. Danehy, S. Roy, Seedless velocimetry at 100 kHz with picosecond-laser electronic-excitation tagging, Optics Letters 42 (2017) 239-242.
[53] N. Calvert, Y. Zhang, R.B. Miles, Characterizing FLEET for aerodynamic measurements in various gas mixtures and non-air environments, 32nd AIAA Aerodynamic Measurement Technology and Ground Testing Conference, Paper No. AIAA-2016-3206, Washington, DC, USA, 2016.
[54] Y.B. Zhang, R.B. Miles, Femtosecond laser tagging for velocimetry in argon and nitrogen gas mixtures, Optics Letters 43 (2018) 551-554.
[55] Y.B. Zhang, M.N. Shneider, R.B. Miles, Femtosecond laser excitation in argon-nitrogen mixtures, AIAA Journal 56 (2018) 1060-1071.
[56] Y.B. Zhang, P.M. Danehy, R.B. Miles, Femtosecond laser tagging in R134a with small quantities of air, AIAA Journal 57 (2019) 1793-1800.
[57] J.B. Michael, M.R. Edwards, A. Dogariu, R.B. Miles, Velocity by femtosecond laser electronic excitation tagging (FLEET) of air and nitrogen, 50th AIAA Aerospace Sciences Meeting, Paper No. 2012-1053, Nashville, Tennessee, USA, 2012.
[58] Y. Zhang, D.R. Richardson, S.J. Beresh, K.M. Casper, M. Soehnel, J. Henfling, R. Spillers, Hypersonic wake measurements behind a slender cone using FLEET velocimetry, AIAA Aviation Forum, Paper No. AIAA-2019-3381, Dallas, Texas, USA, 2019.
[59] L.E. Dogariu, A. Dogariu, R.B. Miles, M.S. Smith, E. Marineau, Femtosecond laser electronic excitation tagging velocimetry in a large-scale hypersonic facility, AIAA Journal 57 (2019) 4725-4737.
[60] D.T. Reese, P.M. Danehy, E.L. Walker, S.M. Rivers, W.K. Goad, FLEET velocimetry in the common research model's wing wake, AIAA SciTech Forum, Paper No. AIAA-2020-1276, Orlando, Florida, USA, 2020.
[61] Y. Zhang, S.J. Beresh, K.M. Casper, D. Richardson, M.M. Soehnel, R.W. Spillers, Tailoring FLEET for cold hypersonic flows, AIAA SciTech Forum, Paper No. AIAA-2020-1020, Orlando, Florida, USA, 2020.
[62] D. Reese, P. Danehy, N.B. Jiang, J. Felver, D. Richardson, J. Gord, Application of resonant femtosecond tagging velocimetry in the 0.3-meter transonic cryogenic tunnel, AIAA Journal 57 (2019) 3851-3858.
[63] R.A. Burns, P.M. Danehy, N.B. Jiang, M.N. Slipchenko, J. Felver, S. Roy, Unseeded velocimetry in nitrogen for high-pressure cryogenic wind tunnels: part II. Picosecond-laser tagging, Measurement Science and Technology 29 (2018) 115203.
[64] J.M. Fisher, M.E. Smyser, M.N. Slipchenko, S. Roy, T.R. Meyer, Burst-mode femtosecond laser electronic excitation tagging for kHz-MHz seedless velocimetry, Optics Letters 45 (2020) 335-338.
[65] S.P. Nandula, R.W. Pitz, J. Bominaar, C. Schoemaecker, N.J. Dam, J.J. ter Meulen, Kinetics of the NO tagging formation in air for unseeded molecular tagging velocimetry, 42nd Aerospace Sciences Meeting, Paper No. AIAA-2004-0390, Reno, Nevada, USA, 2004.
[66] L. Ribarov, J. Wehrmeyer, S. Hu, R. Pitz, Multiline hydroxyl tagging velocimetry measurements in reacting and nonreacting experimental flows, Experiments in Fluids 37 (2004) 65-74.
[67] L.A. Ribarov, J.A. Wehrmeyer, R.W. Pitz, R.A. Yetter, Hydroxyl tagging velocimetry (HTV) in experimental air flows, Applied Physics B-Lasers and Optics 74 (2002) 175-183.

[68] M.A. Andre, P.M. Bardet, R.A. Burns, P.M. Danehy, Characterization of hydroxyl tagging velocimetry for low-speed flows, Measurement Science and Technology 28 (2017) 085202.
[69] R.W. Pitz, M.D. Lahr, Z.W. Douglas, J.A. Wehrmeyer, S. Hu, C.D. Carter, K.Y. Hsu, C. Lum, M.M. Koochesfahani, Hydroxyl tagging velocimetry in a supersonic flow over a cavity, Applied Optics 44 (2005) 6692-6700.
[70] N.R. Grady, R.W. Pitz, C.D. Carter, K.-Y. Hsu, C. Ghodke, S. Menon, Supersonic flow over a ramped-wall cavity flame holder with an upstream strut, Journal of Propulsion and Power 28 (2012) 982-990.
[71] A.N. Perkins, M. Ramsey, D.J. Strickland, R.W. Pitz, J.A. Wehrmeyer, A. Alexander, Dual-pulse hydroxyl tagging velocimetry (HTV) in a jet engine exhaust, 45th AIAA/ASME/SAE/ASEE Joint Propulsion Conference, Paper No. AIAA-2009-5108, Denver, Colorado, USA, 2009.
[72] A. Perkins, N., M. Ramsey, R.W. Pitz, J.A. Wehrmeyer, A.E. Nelius Investigation of a bow shock in a shock tube flow facility using hydroxyl tagging velocimetry, 49th Aerospace Sciences Meeting, Paper No. AIAA-2011-1092, Orlando, Florida, USA, 2011.
[73] J.F. Ye, D.Y. Shi, W.Y. Song, G.H. Li, Z.R. Zhang, Z.Y. Hu, Investigation of turbulence flow characteristics in a dual-mode scramjet combustor using hydroxyl tagging velocimetry, Acta Astronautica 157 (2019) 276-281.
[74] M.C. Ramsey, R.W. Pitz, T.P. Jenkins, Y. Matsutomi, C. Yoon, W.E. Anderson, Planar 2D velocity measurements in the cap shock pattern of a thrust optimized rocket nozzle, Shock Waves 22 (2012) 39-46.
[75] P.T. Tokumaru, P.E. Dimotakis, Image correlation velocimetry, Experiments in Fluids 19 (1995) 1-15.
[76] R.B. Miles, W.R. Lempert, Quantitative flow visualization in unseeded flows, Annual Review of Fluid Mechanics 29 (1997) 285-326.
[77] R. Sanchez-Gonzalez, R. Srinivasan, R.D.W. Bowersox, S.W. North, Simultaneous velocity and temperature measurements in gaseous flow fields using the VENOM technique, Optics Letters 36 (2011) 196-198.
[78] N.R. Grady, Laser Diagnostics of Turbulent Flames in High Speed Flows, Mechanical Engineering Department, Ph.D. Thesis, Vanderbilt University, Nashville, Tennessee, USA, 2015, pp. 110.
[79] B.F. Bathel, C.T. Johansen, P.M. Danehy, J.A. Inman, S.B. Jones, C.P. Goyne, Hypersonic boundary layer transition measurements using NO_2 - NO photodissociation tagging velocimetry, 41st AIAA Fluid Dynamics Conference, Paper No. AIAA-2011-3246, Honolulu, Hawaii USA, 2011.
[80] M.R. Edwards, Femtosecond Laser Electronic Excitation Tagging, Mechanical and Aerospace Engineering, Senior Thesis, Princeton University, Princeton, New Jersey, USA, 2012.
[81] R.B. Miles, M.R. Edwards, J.M. Michael, N.D. Calvert, A. Dogariu, Femtosecond laser electronic excitation tagging (FLEET) for imaging flow structure in unseeded hot or cold air or nitrogen, 51st AIAA Aerospace Sciences Meeting, Paper No. 2013-0340, Grapevine, Texas, USA, 2013.
[82] N.J. DeLuca, R.B. Miles, N.B. Jiang, W.D. Kulatilaka, A.K. Patnaik, J.R. Gord, FLEET velocimetry for combustion and flow diagnostics, Applied Optics 56 (2017) 8632-8638.
[83] R.A. Burns, C.J. Peters, P.M. Danehy, Unseeded velocimetry in nitrogen for high-pressure, cryogenic wind tunnels, part I: femtosecond-laser tagging, Measurement Science and Technology 29 (2018).
[84] C.J. Peters, M.N. Shneider, R.B. Miles, Kinetics model of femtosecond laser ionization in nitrogen and comparison to experiment, Journal of Applied Physics 125 (2019) 243301.
[85] A.E. Lutz, R.J. Kee, J.A. Miller, SENKIN: a FORTRAN program for predicting homogeneous gas-phase chemical kinetics with sensitivity analysis, Sandia National Laboratories, Report No. SAND87-8248, Livermore, California USA, 1988.
[86] J.A. Wehrmeyer, L.A. Ribarov, D.A. Oguss, F. Batliwala, P.A. DeBarber, Flow tagging velocimetry for low and high temperature flowfields, 37th AIAA Aerospace Sciences Meeting, Paper No. AIAA-1999-0646, Reno, Nevada, USA, 1999.
[87] R. Miles, W. Lempert, B. Zhang, Turbulent structure measurements by RELIEF flow tagging, Fluid Dynamics Research 8 (1991) 9-17.
[88] C.M. Limbach, R.B. Miles, Rayleigh scattering measurements of heating and gas perturbations accompanying femtosecond laser tagging, AIAA Journal 55 (2017) 112-120.
[89] J.D. Schmisseur, S.P. Schneider, S.H. Collicott, Supersonic boundary-layer response to optically generated freestream disturbances, Experiments in Fluids 33 (2002) 225-232.
[90] M.R. New-Tolley, M.N. Shneider, R.D. Miles, Modeling of the FLEET filament interaction with a nonuniform gas flow, 55th AIAA Aerospace Sciences Meeting, Paper No. AIAA-2017-0257, Grapevine, Texas, USA, 2017.
[91] M. Mittal, R. Sadr, H.J. Schock, A. Fedewa, A. Naqwi, In-cylinder engine flow measurement using stereoscopic molecular tagging velocimetry (SMTV), Experiments in Fluids 46 (2009) 277-284.
[92] C.P. Gendrich, M.M. Koochesfahani, A spatial correlation technique for estimating velocity fields using molecular tagging velocimetry (MTV), Experiments in Fluids 22 (1996) 67-77.

[93] R. Sanchez-Gonzalez, R.D.W. Bowersox, S.W. North, Simultaneous velocity and temperature measurements in gaseous flowfields using the vibrationally excited nitric oxide monitoring technique: a comprehensive study, Applied Optics 51 (2012) 1216-1228.
[94] M.C. Ramsey, R.W. Pitz, Template matching for improved accuracy in molecular tagging velocimetry, Experiments in Fluids 51 (2011) 811-819.
[95] F. Pan, R. Sanchez-Gonzalez, M.H. McIlvoy, R.D.W. Bowersox, S.W. North, Simultaneous three-dimensional velocimetry and thermometry in gaseous flows using the stereoscopic vibrationally excited nitric oxide monitoring technique, Optics Letters 41 (2016) 1376-1379.
[96] R. Vedula, M. Mittal, H.J. Schock, Molecular tagging velocimetry and its application to in-cylinder flow measurements, Journal of Fluids Engineering-Transactions of the ASME 135 (2013) 1-17.
[97] M.M. Koochesfahani, Molecular Tagging Velocimetry (MTV), in: C. Tropea, A.L. Yarin, J.F. Foss (Eds.), Handbook of Experimental Fluid Mechanics, Springer, Berlin, 2007.
[98] S.J. Kline, F.A. McClintock, Describing uncertainties in single-sample experiments, Mechanical Engineering (1953) 3-8.
[99] R.B. Hill, J.C. Klewicki, Data reduction methods for flow tagging velocity measurements, Experiments in Fluids 20 (1996) 142-152.
[100] M.A. Mustafa, N.J. Parziale, M.S. Smith, E.C. Marineau, Nonintrusive freestream velocity measurement in a large-scale hypersonic wind tunnel, Aiaa Journal 55 (2017) 3611-3616.
[101] G. Hagemann, M. Frey, Shock pattern in the plume of rocket nozzles: needs for design consideration, Shock Waves 17 (2008) 387-395.
[102] D. Edgington-Mitchell, D.R. Honnery, J. Soria, The underexpanded jet Mach disk and its associated shear layer, Physics of Fluids 26 (2014).
[103] D. Bohl, Molecular Tagging Diagnostics, in: R.W. Johnson (Ed.), Handbook of Fluid Mechanics, CRC Press, Boca Raton, Florida USA, 2016.
[104] F. Chen, H.X. Li, H. Hu, Molecular tagging techniques and their applications to the study of complex thermal flow phenomena, Acta Mechanica Sinica 31 (2015) 425-445.
[105] B.R. Halls, N.B. Jiang, J.R. Gord, P.M. Danehy, S. Roy, Mixture-fraction measurements with femtosecond-laser electronic-excitation tagging, Applied Optics 56 (2017) E94-E98.
[106] S. Hu, D.M. Mosbacher, J.A. Wehrmeyer, R.W. Pitz, Simultaneous temperature, species and velocity measurements via combined Raman spectroscopy and HTV, 40th Joint Propulsion Conference, Paper No. AIAA-2004-4167, Fort Lauderdale, Florida, USA, 2004.